Selection of the functional monomer for molecularly imprinted polymers based on cellulosic biomaterial for efficient recognition of Brilliant Green

Karima Ferchichi, Najeh Jaoued-Grayaa, Jihene Kallel, Noureddine Amdouni, Yves Chevalier, Souhaira Hbaieb

Selection of the Functional Monomer for Molecularly Imprinted Polymers Based on Cellulosic Biomaterial for Efficient Recognition of Brilliant Green

Karima Ferchichi[1], Najeh Jaoued-Grayaa[2], Jihene Kallel[1,3], Noureddine Amdouni[1], Yves Chevalier[3] and Souhaira Hbaieb[1,*]

[1] *Laboratoire de Recherche: Caractérisations, Applications et Modélisation de Matériaux, Université de Tunis El Manar, Faculté des Sciences de Tunis, Tunisia.*
[2] *Unité Spécialisée de développement des techniques analytiques, Institut National de Recherche et d'Analyse Physico-chimique, Biotechpole Sidi-Thabet, 2020 Ariana, Tunisia.*
[3] *Laboratoire d'Automatique, de Génie des Procédés et de Génie Pharmaceutique, LAGEPP, Université de Lyon 1, UMR 5007 CNRS, 43 bd 11 Novembre, 69622 Villeurbanne, France.*

* Corresponding author: Souhaira Hbaieb: souhaira.hbaieb@fst.utm.tn
Tel: +216 98 94 74 79 Fax: +216 71 53 76 88

Highlights

- Efficient molecularly imprinted polymer for selective adsorption of Brilliant Green
- Surface coating of Posidonia by thin MIP film allows fast adsorption
- Polyaniline allows strong interactions with Brilliant Green
- Adsorption isotherms on MIPs are modelled by the Langmuir–Volmer model

Abstract. Owing to the demand for chemical analysis of low concentrations of the Brilliant Green (BG) dye released into the environment, molecularly imprinted polymer (MIP) materials have been investigated for their use in SPME preconcentration devices. Thin coatings of MIP on solid supports allow fast adsorption of the analyte and higher selectivity of adsorption. Biosourced fibers of *Posidonia oceanica* (Pos) were taken as solid support to which a thin film of MIP was chemically attached. The material synthesis involved two steps: chemical grafting of methacrylate groups onto Pos by a silane coupling, and copolymerization with the free functional monomer and cross-linker in the presence of BG. Polymerization of the functional monomers methacrylic acid and acrylamide yielded the materials PosMAA@MIP and PosAA@MIP respectively. The strength of their interaction with BG and the stoichiometry of the pre-polymerization complex were assessed by ^{1}H NMR experiments in DMSO-d_6 solution. Characterization by IR spectroscopy and thermogravimetric analysis validated the successful syntheses. The points of zero charge were at pH 3.31 and 4.50 for PosMAA@MIP and PosAA@MIP, respectively, influencing the optimal adsorption of BG at pH 4. Kinetic studies revealed the rapid adsorption of more than 90% of the BG within 20 minutes. All MIPs exhibited higher adsorption capacity for BG compared to non-imprinted materials (NIPs). PosAA@MIP showed the highest adsorption efficiency and selectivity, with an imprinting factor of 1.9. The thermodynamics of adsorption was studied by fitting the Langmuir–Volmer and Volmer models to the experimental data, from which the selective adsorption capacities of BG on PosMAA@MIP and PosAA@MIP were 289 and 313 µmol·g^{-1}, respectively. Additionally, PosAA@MIP exhibited higher extraction efficiency for BG than for its metabolites eosin and methylene blue, underscoring its superior ability to selectively capture target molecules.

Keywords: Brilliant Green, Modified Posidonia, Molecularly Imprinted Polymer, Adsorption, Selectivity.

1. Introduction

Brilliant Green (BG) is a synthetic dye used in various industrial fields with high risk of disposal into the environment. In aquaculture as example, BG has been used as an antifungal and antibacterial agent to control various diseases of fishes and shrimps through selective inhibition of the growth of Gram-positive bacteria [1,2]. However, the use of BG in aquaculture is a matter of concern due to its potential toxicity to aquatic organisms and the risk of accumulation in the food chain [3]. BG has been banned in some countries, including the European Union and the United States, but it is still used in other parts of the world. Consuming fish contaminated with BG residues is a major concern for human health. Exposure to high levels of BG can lead to various adverse health effects including mutagenicity, carcinogenicity and teratogenicity [4]. These risks make monitoring BG residual levels in fish and other seafood products of definite importance to ensure the safety for human consumption. Several methods have been developed for the analysis of BG, including high-performance liquid chromatography (HPLC) coupled with UV absorbance or mass spectrometry detection, gas chromatography-mass spectrometry (GC-MS), and thin-layer chromatography coupled with densitometry [5–9]. These analytical methods typically require a purification step prior to analysis, which is commonly achieved through solid phase extraction (SPE). Purification by SPE aims at increasing their concentration, improving sensitivity, and separating them from interfering compounds that could affect the accuracy of the analysis [10,11]. The target molecules are collected by adsorption onto a solid material; the adsorption should be quantitative to ensure the final concentration is related to the concentration in the collected sample. Selective adsorption is also necessary for accurate analysis at low detection and quantification limits [10]. Despite its effectiveness, the SPE technique suffers from low adsorption capacity and non-selective retention of the analytes. Commonly used SPE cartridges for the determination of toxic substances in fishery products are based on C18 modified silica or polystyrene solid materials that retain analytes by non-specific hydrophobic interactions, leading to co-extraction of many interfering compounds [11]. Molecular Imprinting Technology is a cutting-edge technique extensively used to create highly specific polymeric materials with particular cavities designed to selectively capture a given target molecule [12]. The approach to molecularly imprinted polymers (MIPs) involves the copolymerization of a functional monomer and a cross-linking agent, in which the template molecules are bound to the functional monomer groups via non-covalent interactions. Upon removal of the template molecules from the polymeric matrix, cavities are generated, which are complementary to the template in terms of their size,

functional groups, and shape [13]. These "template-shaped cavities" act as selective recognition sites for the adsorption of template molecules on the surface of MIPs. The most commonly used methods for producing molecularly imprinted polymers (MIPs) are bulk and precipitation polymerization [14]. However, these methods result in MIPs with recognition sites deeply embedded within the polymer matrix, which makes it challenging to extract and rebind the template. To address this issue, surface imprinted MIPs have been proposed to enhance accessibility to the recognition sites formed on the surface of the material during polymerization, leading to improved binding kinetics. Therefore, surface grafting onto solid support surfaces has emerged as a promising surface imprinting technique for producing MIPs with better accessibility to specific binding sites. In this context, the use of natural materials as supports for MIPs has gained interest as a sustainable and cost-effective alternative to traditional synthetic supports. Posidonia fibrous material is a promising alternative as biomaterial support due to its low cost and high availability. Posidonia is a type of marine plant that is composed of cellulose, lignin, and hemicellulose. Its surface is rich in hydroxyl groups, which can be exploited for surface modification. Posidonia grafted with organosilanes containing polymerizable functions has been first prepared. Two different types of monomers, methacrylic acid (MAA) and acrylamide (AA), were selected for investigating the uptake of Brilliant Green by MIPs grafted on Posidonia. Indeed, choosing the appropriate functional monomer with favorable interactions with the template molecule is of utmost importance in molecular imprinting technology. It is recommended to use a functional monomer that has basic functional groups for an acidic template and vice versa. The interaction of BG with the monomers depends on the BG speciation at different pH values (Fig. 1). At acidic pH, BG exists in a protonated form and can interact with the amino group of acrylamide in its neutral form. At basic pH, BG exists as an anion and can interact with an acidic monomer such as methacrylic acid. In both cases, this interaction between BG and monomers through hydrogen bonds and/or electrostatic interactions plays a crucial role in the synthesis of molecularly imprinted polymers. For this study, two different types of MIPs were synthesized using acrylic functional monomers, differing by their acid-base properties. The radical polymerization is initiated with azobisisobutyronitrile (AIBN) initiator in acetonitrile (ACN) as a solvent. The non-imprinted polymers (NIPs) were synthesized under the same conditions as the imprinted polymers but without the template molecule (BG). The adsorption characteristics of the MIPs for BG were examined and compared to their corresponding NIPs to assess their selectivity. Furthermore,

the specificity of the MIPs was evaluated by studying their competitive adsorption behavior with other potentially interfering substances.

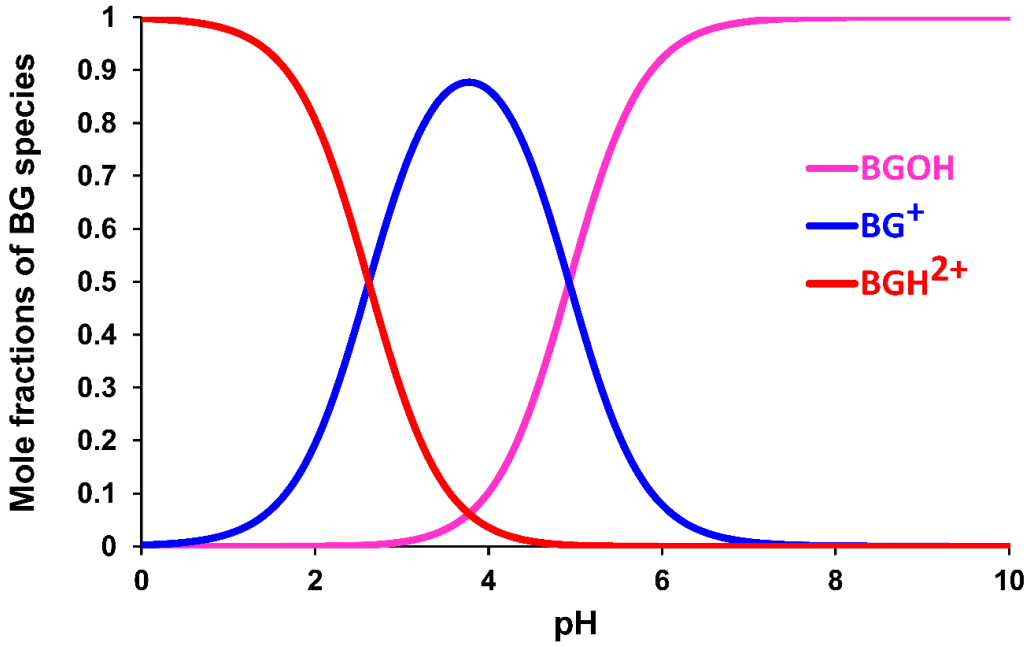

Figure 1. Structure and pH-dependent speciation of Brilliant Green. The graph is plotted using the pK_a values of BG, where BGH^{2+}, BG^+ and BGOH are the different species of BG.

2. Experimental section

2.1. Reagents

γ-Methacryloxypropyltrimethoxysilane (γ-MPTS, 95 %), methacrylic acid (MAA, 99 %), acrylamide (AA, 95 %), azobisisobutyronitrile (AIBN), ethylene glycol dimethacrylate (EGDMA, 98 %) and *N*-ethyldiisopropylamine (≥ 98 %) were purchased from Sigma–Aldrich. HPLC grade acetonitrile (ACN), methanol (MeOH) and tetrahydrofuran (THF) were purchased from Fisher Scientific. Toluene (Fisher Scientific) was distilled before use. Brilliant Green (≥ 98 %), Eosin (≥ 98 %) and Methylene Blue (≥ 98 %) standards were from Sigma–Aldrich. Deuterated dimethylsulfoxide (DMSO-d_6) was obtained from Eurisotop (Saint-Aubin, France) for the NMR experiments. Deionized water with a resistivity of 18 MΩ·cm was utilized for the entire study.

2.2. Methods

IR spectra were recorded with a Bruker IFS 55 Equinox Fourier Transform Infrared spectrometer in ATR mode. Thermogravimetric analyses (TGA) were performed with a TG 209 F1 Netzsch instrument in the temperature range of 25 °C to 800 °C at a heating rate of

10 °C·min^{-1} under a nitrogen flow. Zeta potentials were measured by electrophoresis on 0.05 wt% aqueous suspensions at different pH with a Malvern Zetasizer Nano ZS instrument. The ζ potential was calculated from the electrophoretic mobility under the Smoluchowski approximation. A UV–vis spectrophotometer Varian Cary 50 was used for the absorbance measurements of BG solutions in 1 cm optical path quartz cells. X-ray diffraction (XRD) measurements were performed using a PANalytical X'Pert PRO Multi-Purpose diffractometer working in Bragg–Brentano geometry with Cu Kα radiation at a generator voltage of 45 kV and current of 40 mA.

2.3. Preparation of Posidonia biomaterials

Posidonia oceanica balls were collected from Cheba-Mahdia beach in the east coast of Tunisia. The fibers of biomass balls have been manually separated, extensively washed with large volumes of deionized water for removal of sand and salt coming from sea water and dried in the open air. The obtained Posidonia fibers were washed with ethanol during 24 h in a Soxhlet extractor and dried at 50 °C for 48 h, until the mass of the fibers became constant. The dry biomasses were crushed and sieved so as to recover particles of homogeneous size (50 μm). They were repeatedly washed with deionized water, and dried for 24 h at 50–60 °C. The final Posidonia powders were stored in a desiccator for later use.

2.4. Preparation of the imprinted and non-imprinted materials

The preparation of the imprinted polymers involved a two-step procedure. First, Posidonia (Pos) was modified by grafting γ-MPTS containing anhydrous toluene as solvent and *N*-ethyldiisopropylamine as a catalyst. The mixture was heated at reflux under nitrogen atmosphere for 24 h. The modified Posidonia (Pos@MPTS) was rinsed with 20 mL of THF dried at 60 °C overnight and stored under vacuum for subsequent uses. In the second step (Fig. 2), 1 mmol of BG, 6 mmol MAA or AA monomers and 500 mg of Pos@MPTS in 5 mL of ACN was deoxygenated with a nitrogen gas flow and heated to 70 °C. 6 mmol of EGDMA and 0.2 mmol of AIBN were then added and left for 3 h of polymerization reaction. The resulting material was filtered and washed with methanol. The BG template was then removed using a Soxhlet extractor until no more BG was detected in the washing liquid by UV-visible absorption spectroscopy. The imprinted polymer (MIP) was then dried under vacuum at 60 °C for 24 h. A non-imprinted polymer (NIP) was also prepared using the same procedure as the MIP, but without the addition of Brilliant Green. Table 1 summarizes the various materials synthesized by varying the type of monomer.

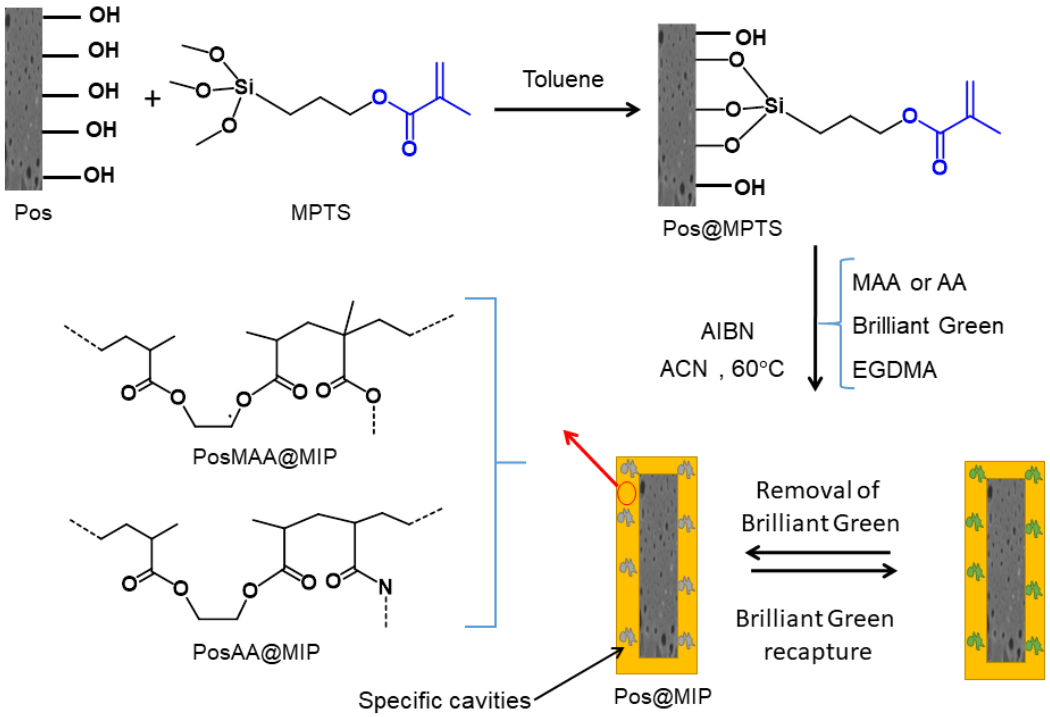

Figure 2. Schematic illustration depicting the synthetic pathway of the second step of the synthesis of molecularly imprinted polymers.

Table 1. List of abbreviations used for the monomers and the synthesized polymer materials.

Monomers	Materials
Methacrylic acid (MAA)	PosMAA@MIP PosMAA@NIP
Acrylamide (AA)	PosAA@MIP PosAA@NIP

2.5. Binding experiments

To investigate the kinetics of Brilliant Green adsorption and determine the equilibrium time, the adsorption process was followed by analyses at various time intervals. A fixed initial concentration of BG aqueous solution at 48.2 mg·L^{-1} was used, and 5 mg of each material was mixed with 10 mL of the prepared solution. The mixture was stirred at 500 rpm during several contact times at room temperature. After each interval, the aliquot was centrifuged at 10000 rpm for 10 min, and the supernatant was filtered through a 0.45 µm RC syringe filter for UV–vis absorption spectroscopy analysis. The absorbance at 624 nm was recorded and used to calculate the concentration of BG in the solution. The adsorbed amount at time t ($Q(t)$, mg·g^{-1}) was calculated using Eq. 1:

$$Q(t) = \frac{V}{m}[C(0) - C(t)] \quad (1)$$

where $C(t)$ (mg·L^{-1}) is the residual BG concentration at time t, $C(0)$ is the initial BG concentration (mg·L^{-1}), V (L) is the volume of BG solution and m (g) is the mass of the material. For adsorption isotherm, the static method was employed by mixing each prepared or non-modified materials (5 mg) with 10 mL of Brilliant Green solution at different initial concentrations varying from 9.64 to 48.2 mg·L^{-1} at room temperature and under continuous stirring for 20 min equilibration time. After equilibration, the mixture was centrifuged and filtered to measure the residual Brilliant Green in the supernatant. The amount of adsorbed BG at equilibrium, Q_e (mol·g^{-1}), was calculated using Eq. 2:

$$Q_e = \frac{V}{m}[C(0) - C(\infty)] \quad (2)$$

where $C(0)$ and $C(\infty)$ are the initial and equilibrium concentrations of Brilliant Green solutions, respectively, V is the volume of Brilliant Green solutions and m is the mass of the used material. The imprinting efficiency of the MIP was determined using the following Eq. 3:

$$IF = \frac{Q_e(\text{MIP})}{Q_e(\text{NIP})} \quad (3)$$

where Q_e(MIP) (mol·g^{-1}) and Q_e(NIP) (mol·g^{-1}) are the adsorbed quantities of BG at equilibrium for the MIP and NIP respectively [15].

2.6. Adsorption isotherm modeling

To investigate the adsorption mechanism and affinity of Brilliant Green towards the adsorbents, adsorption isotherm models were employed. The Langmuir–Volmer model [12] was utilized due to its ability to model the simultaneous adsorption on and off the molecular imprints present in the MIPs. This model combines the localized selective adsorption process to molecular imprints described by the Langmuir model (subscript s), and the non-selective adsorption as a mobile adsorbed layer described by the Volmer model (subscript ns). The Volmer model was used to describe Brilliant Green adsorption onto non-imprinted polymers.

The subsequent equations outline the Langmuir and Volmer models, accordingly (Eq. 4)).

$$C = \frac{1}{K_{ns}} \frac{\theta}{1-\theta} e^{\frac{\theta}{1-\theta}} \quad (4)$$

where θ is the surface coverage, $\theta = \frac{Q_{ns}}{Q_{max,ns}}$ and K_{ns} is the binding constant for adsorption equilibrium.

$$Q_s = Q_{max,s} \frac{K_s C}{1+K_s C} \quad (5)$$

where C is the equilibrium concentration of Brilliant Green. $Q_{max,s}$ is the maximum adsorption capacity. K_s is the Langmuir binding constant.

2.7. NMR study

^{1}H NMR spectra were obtained using a Bruker AV500 spectrometer working at 500 MHz Larmor frequency. Firstly, ^{1}H NMR spectra were recorded in DMSO-d_6 for mixtures of a constant concentration (12 mM) of the template molecule (T) and varying ratios (ranging from 1/4 to 1/12) of the monomer molecule (M) to assess their interactions. The two compounds were mixed together in solution and stirred for 1 h to allow for the formation of the pre-polymerization complex. The chemical shifts of the protons (Ha, Hb, Hc, Hd, He, Hf and Hg) of the template molecule were measured as a function of the increasing concentration of the monomer molecule (Table S1). Secondly, The stoichiometry of the template-monomer complex (T:M) is determined by measuring the chemical shift differences ($\Delta\delta$) in ^{1}H NMR between mixed template-monomer solutions and solutions of pure compounds (either template or monomer) [16,17]. Two series of equimolar samples containing template molecule (T) and the monomer molecule (M) were prepared in DMSO-d_6. The total concentration of the two species, (T) and (M), was kept constant for each solution, and the mole ratio (r) was varied from 0 to 1. The mole fraction of (T) is defined as r = [T]/([T] + [M]), and for the monomer (M), r = [M]/([T] + [M]). Thus, the total concentration ($[T]_t + [M]_t$) is equal to 26.16 mM. The samples were stirred during 1 h for the formation of the complex in pre-polymerization medium.

The association of T and M is a reversible process that can be described by the following Eq. 6:

$$m\,T + n\,M \leftrightarrows T_m{:}M_n \tag{6}$$

The overall association constant is written in its general form as follows:

$$\beta_{mn} = \frac{[T_m{:}M_n]}{[T]^m[M]^n} = \frac{[T_m{:}M_n]}{([T]_t - m[T_m{:}M_n])^m([M]_t - n\,[T_m{:}M_n])^n} \tag{7}$$

The mole ratio r of BG is expressed by:

$$r = \frac{m}{m+n} \qquad (0 < r < 1) \tag{8}$$

To determine the association constants between template molecule (T) and functional monomers (M), non-linear regressions of 1:1 (K_1) or 1:2 (K_2) association models were used to determine the association constants from experimental chemical shifts. The 1:1 association model represents a simple equilibrium in which Brilliant Green (T) and a monomer (M) associate to form a new species (T:M).

$$T + M \leftrightarrows T{:}M \qquad K_1 = \frac{[T{:}M]}{[T][M]} \tag{9}$$

with $[T]_{tot} = [T] + [T{:}M]$ and $[M]_{tot} = [M] + [T{:}M]$.

When the exchange between the free and associated Brilliant Green molecules is fast, the chemical shift (δ) of each NMR resonance is a weighted average of the chemical shifts of the free (δ_T) and associated ($\delta_{T:M}$) molecules as shown in Eq. 10.

$$\delta = \frac{[T]}{[T]_{tot}}\delta_T + \frac{[T:M]}{[T]_{tot}}\delta_{T:M} \quad (10)$$

Solving the above equations gives Eq. 11:

$$[T:M] = \frac{1}{2}\left[[T]_{tot} + [M]_{tot} + \frac{1}{K_1} - \sqrt{\left([T]_{tot} + [M]_{tot} + \frac{1}{K_1}\right)^2 - 4[T]_{tot}[M]_{tot}}\right] \quad (11)$$

The formation of a complex ($T:M_2$) between the template (T) and the monomer (M) is described by the following equilibria (Eqs. 12 and 13) [17,18]:

$$T + M \leftrightarrows T:M \qquad K_1 = \frac{[T:M]}{[T][M]} \quad (12)$$

$$T:M + M \leftrightarrows T:M_2 \qquad K_2 = \frac{[T:M_2]}{[T:M][M]} \quad (13)$$

The overall (cumulated) complexation constant β_2 is defined as a combination of the complexation constants K_1 and K_2 as depicted in Eq. 14:

$$\beta_2 = K_1K_2 = \frac{[T:M_2]}{[T][M]^2} \quad (14)$$

The calculation of [T], [M], [T:M] and [$T:M_2$] is done by solving the third-degree Eq. 15:

$$K_1K_2[M]^3 + [M]^2[K_1 + K_1K_2(2[T]_{tot} - [M]_{tot})] + [M][1 + K_1([T]_{tot} - [M]_{tot})] - [M]_{tot} = 0 \quad (15)$$

which fills up the form as expressed in the form of Eq. 16:

$$\alpha x^3 + \beta x^2 + \gamma x + \delta = 0 \quad (16)$$

with $x = [M]$ such as: $\alpha = 1$ (16a)

$$\beta = \frac{K_1 + K_1K_2(2[T]_{tot} - [M]_{tot})}{K_1K_2} = \frac{1}{K_2} + 2[T]_{tot} - [M]_{tot} \quad (16b)$$

$$\gamma = \frac{1 + K_1([T]_{tot} - [M]_{tot})}{K_1K_2} \quad (16c)$$

$$\delta = \frac{[M]_{tot}}{K_1K_2} \quad (16d)$$

2.8. Competitive binding experiments

Eosin and Methylene blue were selected as interfering species to assess the selectivity of the MIP materials. These molecules were chosen because of their similar structure to Brilliant Green and their high frequency of occurrence together in the water of aquaculture ponds. 5 mg of the adsorbent was immersed in 10 mL of aqueous solutions containing 10 mg·L^{-1} of Brilliant Green, Eosin and Methylene blue. After stirring for 20 min at 500 rpm and at room temperature, the residual concentration in the supernatant was analyzed by UV–vis at the wavelength of maximum absorbance of each molecule (Brilliant Green (BG): λ_{max} = 624 nm), (Eosin (Eos):

λ_{max} = 520 nm) and (Methylene blue (MB) = 664 nm). The determination of the extraction efficiencies (*ee*) of BG and its analogs consisted of measuring the equilibrium concentration (C_e) in the supernatant and the initial concentration of the analyte $C(0)$ according to the following equation:

Extraction Efficiency (%): $ee = \frac{100}{C(0)}(C(0) - C_e)$ (17)

The selectivity of the adsorbent was evaluated by determining the distribution coefficient (*D*, $L \cdot g^{-1}$) and the selectivity coefficient (α) using the parameters described in Eqs. 18 and 19. The distribution coefficient was the ratio of the adsorbed quantity at equilibrium to the adsorbate concentration remaining in solution at equilibrium for each substance.

$$D = \frac{Q_e}{C_e} \quad (18)$$

The selectivity coefficient α was calculated by Eq. 19:

$$\alpha = \frac{D_{\text{analyte,MIP}}}{D_{\text{competitor,MIP}}} \quad (19)$$

where $D_{\text{analyte,MIP}}$ and $D_{\text{competitor,MIP}}$ are respectively the distribution coefficients for the matrix template and for the competing molecules.

3. Results and discussion

3.1. Synthesis and characterization of imprinted materials

Posidonia biomaterial possesses several surface functional groups, which are easily employed as grafting sites. The preparation of MIPs was achieved in two synthetic steps: γ-MPTS containing acrylic group was firstly grafted onto the Posidonia surface to provide Pos@MPTS with anchored acrylic monomers available for subsequent copolymerization. The silane coupling agent was covalently attached to the Posidonia surface by the reaction of functional groups present at the surface of Posidonia with the methoxy groups of γ-MPTS [19,20]. The acrylic groups in γ-MPTS modifier have strong reactivity and can effectively induce and participate to the radical polymerization of free monomers. The resulting Pos@MPTS material was characterized by IR spectroscopy and thermogravimetric analysis. The results are given in Figs. S1 and S2 of the SI file. The selection of the polymerization method is crucial for the preparation of a highly selective imprinted polymer. Surface imprinting polymerization was preferred over the traditional bulk polymerization method due to several advantages it offers. This technique can enhance the molecular recognition capability between the polymer and target molecule during the adsorption process by creating imprinting sites on the outer layer of

the polymer based on the substrate. It can also improve the mass transfer kinetics and eliminate the problem of incomplete template removal. The surface imprinting technique of grafting polymerization synchronized with cross-linking imprinting has been chosen as the polymerization strategy due to its benefits over traditional methods. This method involves two processes: (1) the formation of a pre-polymerization complex between Brilliant Green and the monomer, and (2) the use of the methacrylic group on the surface of Pos@MPTS and an added initiator to induce monomer-Brilliant Green pre-polymerization medium and cross-linking EGDMA to create a layer of copolymer on the surface of modified Posidonia, trapping Brilliant Green molecules in the cross-linked networks. In addition, a self-assembly approach utilizing non-covalent interactions between the template and monomer, such as hydrogen bonds, hydrophobic, and van der Waals forces, was employed for molecular imprinting. This approach is common for the production of imprinted polymers due to its ease in preparing the template-monomer complex, simplicity in removing the template, and ability to generate imprinted polymers with strong binding affinity [21]. Selecting the right functional monomer is crucial for the formation of a stable template-monomer complex in the pre-polymerization medium, and to create template-specific sites during the polymer imprinting process. Thus, the Brilliant Green molecule, which contains a nitrogen atom and an aromatic ring, can easily participate in hydrogen bonds and π-electron interactions. MAA is a functional monomer that is commonly used due the hydrogen bond acceptor and donor properties of its carboxylic acid group. Similarly, AA was chosen for its ability to exhibit strong hydrogen bonding interactions with a variety of template molecules [17,22,23]. Acetonitrile was a favorable solvent for non-covalent interactions while not compromising the radical polymerization process [24]. The imprinted and non-imprinted materials were both characterized by IR spectroscopy, TGA and DRX measurements. The IR spectra of the imprinted and non-imprinted polymers exhibited comparable characteristic bands (Fig. 3), indicating similar chemical compositions as expected given their similar polymerization components. According to the IR spectra, the extraction process removed BG from the MIP materials to completion since there was no discernible difference between the IR spectra of NIP and MIP. The IR spectra of NIP and MIP materials revealed a band at 1670 cm^{-1} for materials synthesized with the AA monomer and at 1720 cm^{-1} for materials synthesized with the MAA monomer, which corresponded to the stretching vibrations of their C=O bonds. A band at 2900 cm^{-1} assigned to the stretching vibrations of C–H of $–CH_3$ and $–CH_2$ in EGDMA, AA and MAA showed that EGDMA effectively cross-linked MAA and AA at the surface of Pos@MPTS.

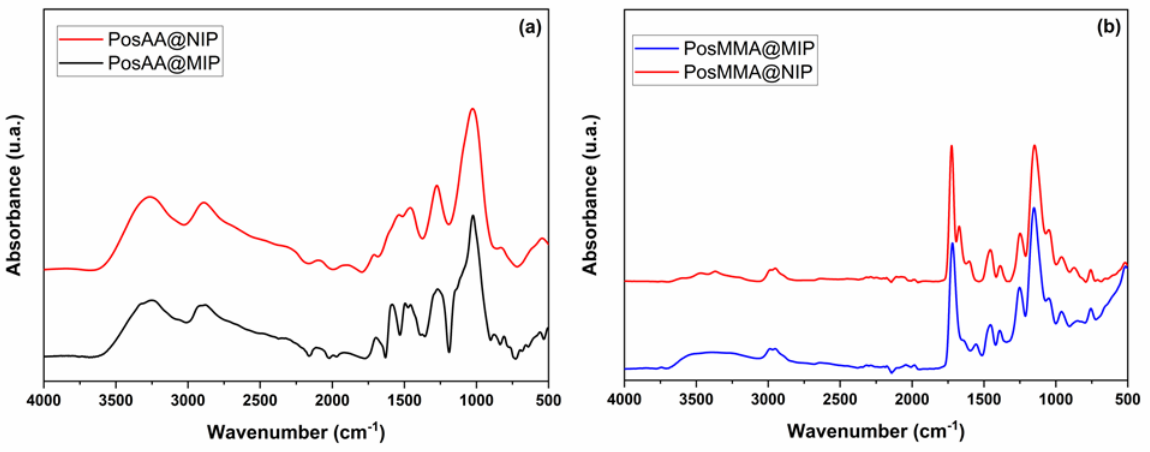

Figure 3. IR spectra of (a) PosAA@MIP and PosAA@NIP, (b) PosMAA@MIP and PosMAA@NIP.

Thermogravimetric analysis was employed to determine the grafting density of the materials. The TGA patterns of the imprinted and non-imprinted polymers exhibited similar trends (Fig. 4). The initial stage of the TGA curves, between 100–200 °C, revealed a mass loss of approximately 10 %, corresponding to the desorption of adsorbed water. The subsequent stage, spanning over 250–450 °C, showed a significant mass loss attributed to the thermal decomposition of the polymer coatings. Notably, the decomposition of the polymer material occurred in multiple steps for PosMAA@MIP and PosAA@MIP.

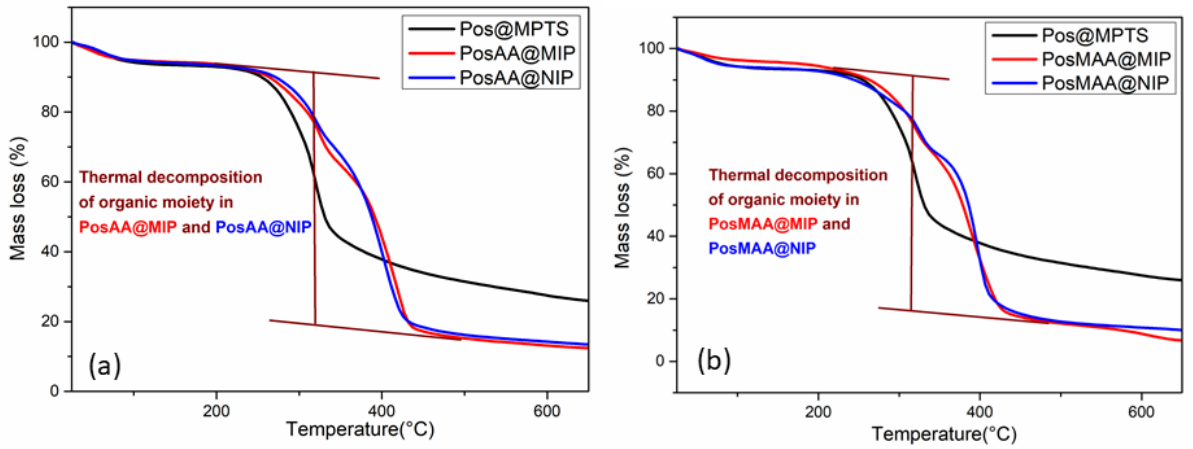

Figure 4. Thermogravimetric analysis of Pos@MPTS, (a) PosAA@MIP and PosAA@NIP, (b) PosMAA@MIP and PosMAA@NIP.

The determination of the grafting densities was carried out using Eq. 20:

$$Surface\ grafting\ density = \frac{M(\text{Pos@copolymer}) - M(\text{ Pos@MPTS})}{100 \times M_{\text{mol}}(\text{grafted copolymer})} \quad (20)$$

where M(Pos@copolymer) is the mass loss of Pos@copolymer, M(Pos@MPTS) is the mass loss of Pos@MPTS, and M_{mol}(grafted copolymer) is the molar mass of the average repeat unit of grafted monomer/cross-linker 50/50 copolymer.

The grafting densities of all materials were similar (Table 2), which was expected for MIP and NIP prepared with the same reagents. MAA and AA-based materials also had the same grafting densities of comparable magnitude with reports in the literature [20].

The differences in final mass among Pos@MPTS, PosAA@MIP, PosAA@NIP, PosMAA@MIP and PosMAA@NIP can be attributed to variations in the degrees of mass loss during the decomposition of the materials. Pos@MPTS, serving as a reference, exhibited a lower mass loss compared to the imprinted and non-imprinted polymers. The higher mass loss in PosMAA@MIP, PosMAA@NIP, PosAA@MIP and PosAA@NIP indicated the decomposition of the polymer matrix and the grafted components. The grafting densities were similar for both MIP and NIP materials, as expected since they were prepared with the same type and amount of reagents. The determined grafting densities, derived from the mass loss data, confirmed the successful grafting of polymers onto the biomaterial Posidonia.

Table 2. Mass losses from TGA and corresponding grafting densities, and pH at the point of zero charge (PZC).

Materials	Mass loss (%)	Grafting density ($mmol \cdot g^{-1}$)	pH_{PZC}
Pos@MPTS	54.7	5.6	2.15
PosMAA@MIP	74.2	54.4	3.31
PosMAA@NIP	74.8	54.6	–
PosAA@MIP	72.2	54.4	4.50
PosAA@NIP	72.1	54.6	–

The pH plays a crucial role in the adsorption process as it greatly influences the surface charge of the adsorbent and the molecular structures of the adsorbates, thereby affecting the adsorption capacity. To understand the impact of the surface charge on the adsorption of BG molecules, the zero charge or pH at the point of zero charge (pH_{PZC}) was determined for each material. The pH_{PZC} represents the pH value at which the resultant positive and negative charges on the surface of the material cancel out. This parameter is particularly important in adsorption phenomena involving electrostatic forces, as is the case with acrylic polymers. The pH_{PZC} values were determined by measuring the zeta potential using suspensions of the materials in ultra-pure water and adjusting the pH (ranging from 2 to 10) by adding 0.1 M NaOH or HCl

solution. The suspensions were kept under constant agitation at room temperature for 4 hours to reach the final pH. Both MIP and NIP materials showed identical behavior. The isoelectric point was *iep* = 6.7, departing a lot from the isoelectric point of bare silica (*iep* ≈ 2).Based on the zeta potential measurements of the PosAA@MIP and PosMAA@MIP materials as a function of pH (Fig. 5), the isoelectric points were determined to be pH 3.31 and pH 4.50, respectively. These values are significantly different from the isoelectric point of Posidonia at pH 2.15. Furthermore, the overall surface charge of the adsorbent is negative for pH values above the respective isoelectric points. The prepared materials contain polar functional groups, and the electrical charge of the adsorbent is pH-dependent due to the ionization of these surface functional groups.

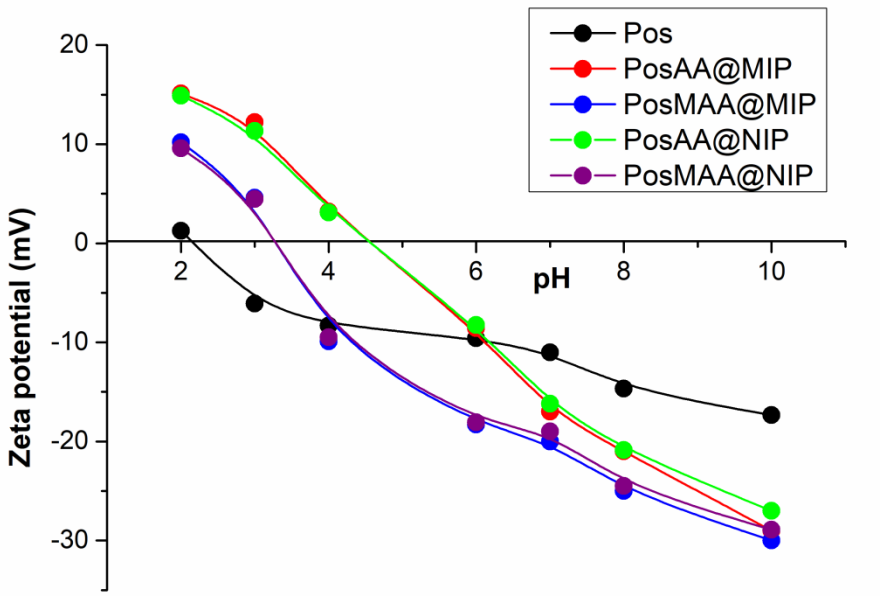

Figure 5. Zeta potential measurements of Pos, PosAA@MIP, PosAA@NIP, PosMAA@MIP and PosMAA@NIP as a function of pH.

The crystalline structure of Pos, PosAA@NIP and PosAA@NIP samples are investigated by using XRD (Fig. 6). The same four characteristic Bragg peaks were detected for all samples at around 15 °, 16 °, 22 ° and 34.5 ° assigned to planes of $\bar{1}10$, 110, 200 and 004, respectively of the monoclinic lattice of type I cellulose [25]. The peak observed in the Pos pattern at $2\theta = 29°$ is attributed to mineral impurities that are largely present in sea biomass [26]. All XRD patterns showed a strong background decaying at high scattering angles. Such large scattering is not observed with pure cellulose, so that it was predominantly ascribed to the amorphous lignin part of Posidonia fibers, and to a lower extend to the amorphous part of semi-crystalline cellulose. The determination of the crystalized fraction of cellulose (crystallinity index) is tricky

with pure cellulose [27,28]. It is even more difficult and hazardous in the presence of a strong background coming from a supplementary phase. Subtraction of this background would require its experimental measurement on a reference sample that is not available. The determination of the crystallinity indices were not attempted because of such an uncertainty regarding the background level. It was nevertheless obvious at qualitatively looking at the XRD patterns that the pristine Posidonia was not crystalline than the PosAA and PosMAA. The synthesis of the MIP materials at the surface of Posidonia fibers was a chemical treatment that decreased the crystallinity of cellulose. This treatment kept (did not extract) the amorphous phase of lignin because the background signal was the same for Pos, PosAA and PosMAA. The loss of cellulose crystallinity was higher in PosMAA than PosAA. The acidic nature of methacrylic acid probably broke the hydrogen bonds responsible for the stability of the cellulose crystalline phase.

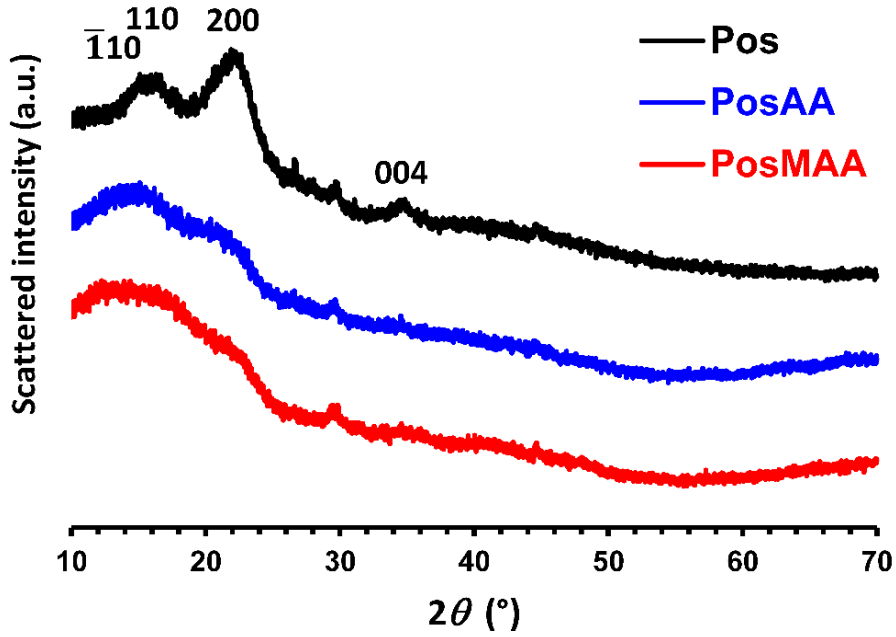

Figure 6. XRD patterns of Pos, PosAA@NIP and PosMAA@NIP.

3.2. Evaluation of the recognition properties the imprinted materials

The adsorption behavior is the primary criterion for evaluating the performance of MIPs. Adsorption isotherms have been measured by the depletion method. The difference in adsorbed amounts between the MIP and NIP materials is an evidence for the presence of molecular imprints. Equilibrium adsorption isotherms provide a thermodynamic perspective on interactions occurring both at and away from the molecular imprints and allow quantitative assessment of the role of different functional monomers on adsorption performance.

3.2.1. Effect of pH

The adsorption behavior depends on the pH for acidic or basic molecules (including Brilliant Green) experiencing several ionization states according to the pH. A strong pH dependence of the surface properties of polyacrylamide is not expected since the neutral primary amide units in its cross-linked structure do not possess notable acidic or basic characteristics in water. Conversely, poly(methacrylic acid) exhibits pronounced pH-dependent behavior due to the presence of ionizable acidic protons in its structure. Therefore, the adsorption of poly(methacrylic acid) onto various surfaces will be notably affected by the pH of the surrounding environment. Moreover, the high polarity and solubility of Brilliant Green make it highly mobile. The adsorption of Brilliant Green on adsorbents is significantly influenced by its ionization behavior. Brilliant Green contains multiple amino ionizable functional groups and exhibits ionization behavior depending on the pH conditions [29]. Under acidic, neutral, and alkaline conditions, Brilliant Green can exist as cationic, zwitterionic, or anionic species, respectively. Therefore, the adsorption of Brilliant Green onto Pos, PosMAA@MIP, PosAA@MIP, and other materials is expected to be greatly influenced by its ionization behavior. The adsorption behavior of Brilliant Green was examined under four distinct pH conditions: 2, 4, 6 and 8 (Fig. S3). Interestingly, the adsorption of Brilliant Green showed its highest favorability at pH 4.

3.2.1. Adsorption kinetics

The materials were designed with a thin polymer coating grafted onto the surface of the Posidonia biomaterial support. This surface molecularly imprinted polymer (MIP) technology ensured excellent accessibility to the molecular imprints, resulting in fast adsorption kinetics.

The adsorption process exhibited two distinct phases: an initial rapid adsorption phase lasting less than 5 min, followed by a slower adsorption phase. Equilibrium adsorption was reached within 20 min, as indicated by the plateau observed in the adsorption kinetics (Fig. 7). As expected, the imprinted materials MIP showed higher adsorption capacities than the non-modified Pos and non-imprinted materials NIP. The initial fast adsorption phase accounted for approximately 90 % (PosMAA@MIP) to 95 % (PosAA@MIP) of the total adsorption. The fast kinetics can be attributed to the presence of the imprinted coating layer and the high specific surface area of the Posidonia support, which facilitates efficient mass transfer and reduces diffusion time [12]. These findings are consistent with a comparative study that demonstrated the rapid adsorption kinetics of a surface-imprinted polymer for gossypol compared to a traditionally prepared bulk-imprinted polymer [12,30]. Thus, early molecularly imprinted

polymers were created using polymer beads produced through radical polymerization in the presence of a porogen. The intention behind the porous structure was to offer a large and accessible specific surface area, ensuring a substantial binding capacity [31]. However, a drawback for certain applications was the relatively slow binding kinetics due to the small pore sizes. According to limited experimental data, the typical timeframe ranged from 1 hour to several days. These characteristics were similar to materials prepared through sol-gel processes, mesoporous materials [32], and by aggregation of colloidal nanoparticles [33,34] in which pores are interstices between primary particles. Instances of rapid adsorption were observed when the pores were of larger sizes [35]. Hence, the present fast adsorption kinetics came from the favorable porosity of the solid support and the thin thickness of the active MIP layer, in accordance with literature data.

The rapid mass transfer rate observed in the MIPs is advantageous for sample pre-concentration applications, such as solid-phase extraction, as it reduces the analysis duration. Furthermore, it was observed that the adsorption kinetics on the imprinted materials were comparable to those on the non-imprinted materials, indicating that the kinetics are mainly controlled by acrylic polymers grafted onto Posidonia support. In all cases, the Brilliant Green adsorption capacities of the imprinted polymers were higher than those of their corresponding non-imprinted counterparts.

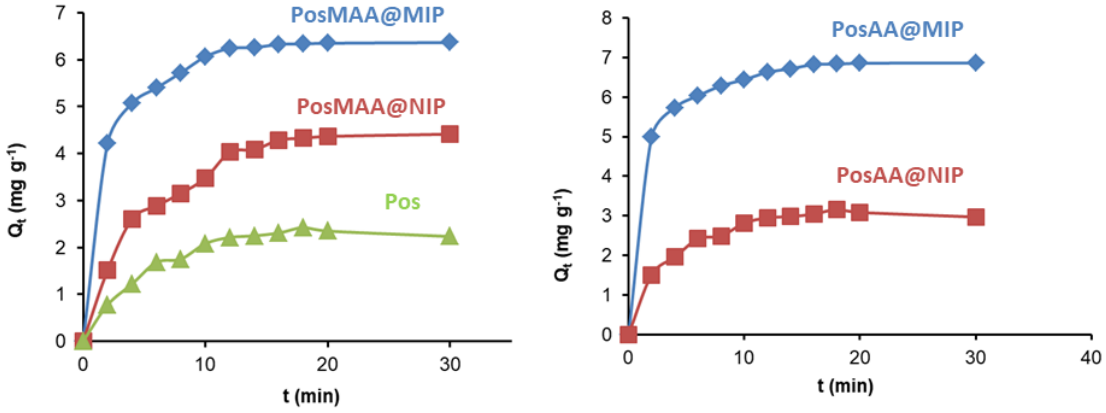

Figure 7. Impact of contact time on the adsorption capacity of Brilliant Green at a concentration of 10^{-5} mol·L^{-1} onto Pos, PosMAA@MIP, PosMAA@NIP, PosAA@MIP, and PosAA@NIP at 298 K and pH 4.

3.2.2. Adsorption isotherms

Equilibrium adsorption isotherms were measured for Pos, MIPs and NIPs over a wide range of concentrations, and models were fitted to the experimental data. Fig. 8 depicts the adsorption

isotherms of Brilliant Green on Pos, MIP and NIP materials, which exhibit a typical shape. The adsorbed amount of Brilliant Green increases with the initial concentration and reaches a plateau at higher concentrations, indicating that all the adsorption sites are occupied and the surface is fully covered by adsorbed Brilliant Green molecules. Non-selective interactions were assessed by conducting adsorption measurements on NIPs. A clear distinction in adsorption behavior between MIPs and NIPs can be observed in MIP-related studies. The "Imprinting Factor" (*IF*) is defined as the ratio of adsorption between MIP and NIP, which indicates the degree of selective adsorption to molecular imprints. Notably, the MIPs exhibit higher adsorption capacity than the NIPs, indicating the presence of specific imprinted sites in addition to the available surface for non-specific adsorption. To describe the adsorption equilibrium, thermodynamic models were employed, involving binding constants and maximum adsorbed amounts. Visual examination of the experimental adsorption isotherms alone is not sufficient to determine the adsorption capacity and affinity of the materials. Models are necessary for a quantitative comparison of material properties. The Langmuir isotherm model is used to describe adsorption on localized molecular imprints, while the Volmer isotherm model is used for non-selective mobile adsorption [12]. The Langmuir model is favored for its compatibility with low temperatures and ease of use in environmental adsorption studies. It assumes monolayer adsorption without intermolecular interactions and provides a clear interpretation. However, limitations arise from the reliance on assumptions and the neglect of intermolecular interactions. The applicability of the model is limited at non-constant temperatures. In the case of non-localized binding with lateral diffusion on the surface, the Volmer model accurately describes this physicochemical mechanism. The Langmuir–Volmer adsorption isotherm was used to model adsorption on the MIP, while the Volmer adsorption model was used for the NIP. The theoretical adsorption isotherms were fitted to the experimental data using the average relative error function (*ARE*) as a criterion for minimizing the error.

$$ARE = \frac{1}{(N-p)} \sum_{i=1}^{N} \left| Q_{\mathrm{exp},i} - Q_{\mathrm{calc},i} \right| \qquad (21)$$

with N and p being respectively the number of data points and fitted parameters, Q_{exp} and Q_{calc} are the experimental and theoretical adsorbed quantities at equilibrium.

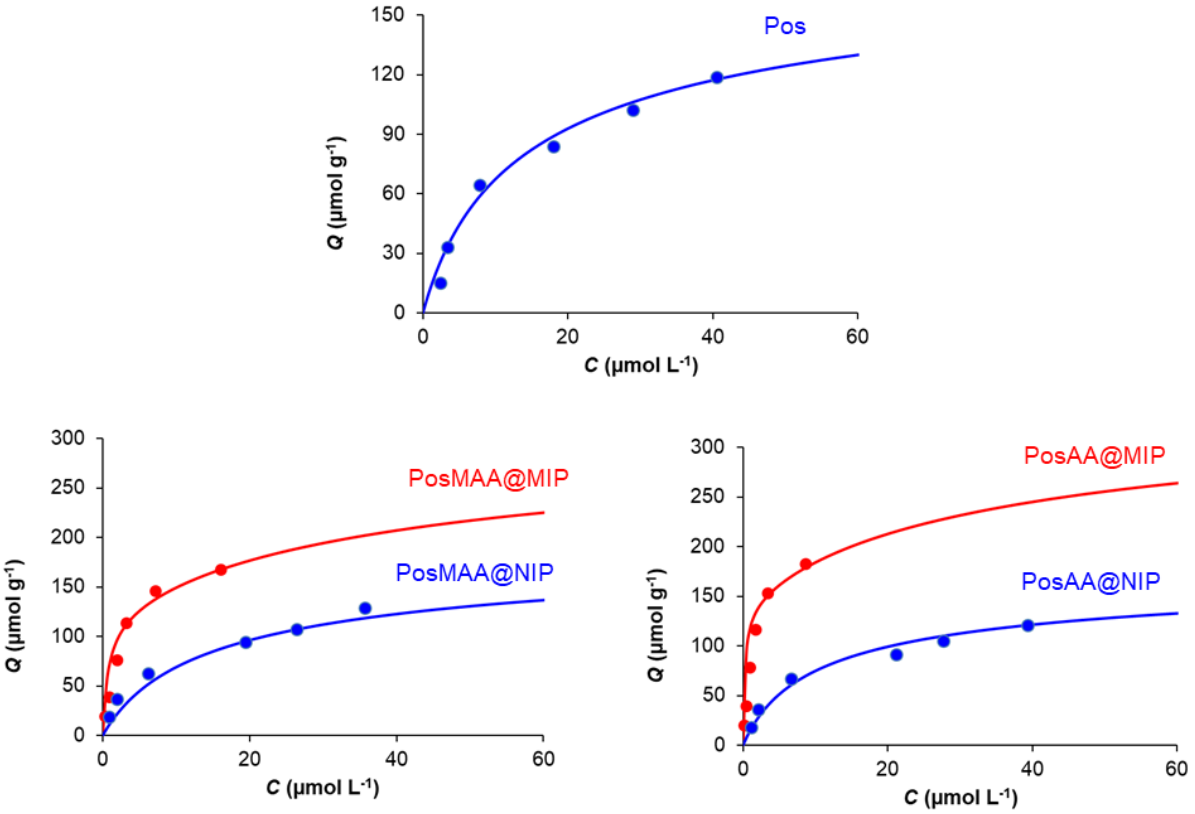

Figure 8. Experimental adsorption isotherms and best fits of the adsorption models for adsorption of Brilliant Green onto Pos, PosMAA@MIP, PosMAA@NIP, PosAA@MIP and PosAA@NIP at 298 K and pH 4.

Selective adsorption on molecular imprints is described by the parameters $Q_{max,s}$ and K_s of the Langmuir model and the parameters $Q_{max,ns}$ and K_{ns} of the Volmer isotherm correspond to non-selective adsorption. The good fit of the adsorption models to the experimental data (Fig. 8) with low values of *ARE* provided the parameters of the Langmuir and Volmer isotherms shown in Table 3. Notably, the two different functional monomers were able to produce selective molecular imprints. Among the tested materials, PosAA@MIP demonstrated the highest affinity for BG. It exhibited both the highest selective and total adsorption capacity (respectively $Q_{max,s}$ and $Q_{max,s} + Q_{max,ns}$). This enhanced binding ability was attributed to the presence of hydrogen bonding interactions between BG and AA. At pH 4, BG exists in its zwitterionic form, with both positive and negative charges. The amino groups of BG can form hydrogen bonds with the carbonyl groups of AA, resulting in strong attractive interactions between the two molecules. Additionally, hydrophobic interactions may also contribute, as the aromatic ring of BG can interact with the hydrophobic regions of AA. These combined interactions enhance the binding affinity and selectivity of PosAA@MIP for BG at pH 4. In the case of MAA, hydrogen bonding can occur between MAA and Brilliant Green. MAA is a weak

acidic monomer that can undergo ionization and exhibit hydrogen bonding properties. MAA can also form hydrogen bonds with BG through interactions between the carboxyl groups of MAA and the amino groups of BG. The equilibrium constants K_s (for molecular imprints in MIPs) are higher than the K_{ns} (for NIPs) for both materials, demonstrating a higher affinity of the molecular imprints for BG compared to non-selective adsorption. In all cases, a difference is observed between $Q_{max,ns}$(MIP) and $Q_{max,ns}$(NIP) (Table 3), which could be attributed to the presence of selective sites that may have been damaged during the template extraction or grinding process, converting specific adsorption sites into non-specific areas. In conclusion, a wide range of functional monomers can be used to prepare MIPs for BG at different pH, the MIP technology enables the creation of selective molecular imprints. Therefore, the PosAA@MIP material exhibited the highest efficiency among the prepared materials, as indicated by its highest adsorption capacity and the largest difference in adsorption capacities between the MIP and NIP materials, quantified by the imprinting factor (*IF*) of 1.9, compared to an *IF* of 1.5 for PosMAA@MIP. The high adsorbed fraction (98 %) demonstrated the efficacy of using the monomer AA for the synthesis of the polyacrylamide MIP materials.

Table 3. Parameters of the Volmer and Langmuir–Volmer models fitting to experimental adsorption isotherms of Brilliant Green onto non-modified, NIP and MIP materials at 298 K and pH 4.

Materials	Non-selective adsorption		Selective adsorption		*ARE*
	$Q_{max,ns}$ ($\mu mol \cdot g^{-1}$)	$\log(K_{ns})$	$Q_{max,s}$ ($\mu mol \cdot g^{-1}$)	$\log(K_s)$	
Pos (Volmer)	250.21	4.72	–	–	0.18
PosMAA@NIP (Volmer)	268.45	4.68	–	–	0.23
PosMAA@MIP (Langmuir–Volmer)	288.81	4.26	140.28	6.14	0.14
PosAA@NIP (Volmer)	240.13	4.85	–	–	0.09
PosAA@MIP (Langmuir–Volmer)	312.86	4.32	118.11	6.62	0.07

3.3. NMR study of Template-Monomer interactions in the pre-polymerization medium

The initial stage in the successful creation of molecular imprints involves the formation of a "pre-polymerization complex" between the template molecule and the functional monomer. Therefore, the choice of the functional monomer can be determined by evaluating these interactions in solution within the polymerization medium. The assessment of template-monomer interactions using ^{1}H NMR spectroscopy provided valuable insights into the optimal

M/BG ratio for the preparation of molecularly imprinted polymers [12,36,37]. To investigate the interactions between the template molecule (BG) and the functional monomer (M), ^{1}H NMR spectra of BG with varying concentrations of M in DMSO-d_6 solution were recorded to evaluate the pre-polymerization mixtures and determine the optimal BG/M ratio for MIP preparation. Spectra were compared at different BG/M molar ratios ranging from 4 to 12, and the corresponding pure BG, MAA and AA spectra were used as references (Figs. S5, S6 and S7 in the SI file). Significant chemical shift variations were observed in all BG protons Ha, Hb, Hc, Hd, He, Hf and Hg (Fig. S4) in the presence of AA (Fig. 9 and Table S1) or MAA (Fig. S8 and Table S2). These shifts were towards the high-field region of the spectrum, indicating an interaction between BG and AA or MAA. The largest shift was observed for Hf AA protons adjacent to the amino group, suggesting the formation of hydrogen bonds between the BG amino groups and the amino group of AA or the carboxylic acid groups of MAA. The magnitude of the shifts increased with increasing BG/AA or BG/MAA mole ratio from 4 to 8, indicating a higher degree of complex formation with higher amounts of monomer. However, for the BG/AA or BG/MAA mole ratios of 10 and 12, there was a decrease in the magnitude of the chemical shift variations, suggesting a decrease in the formation of complex species with higher amounts of monomer. Furthermore, it is crucial to strike a balance between the quantity of functional monomer and cross-linker used. An excessive amount of monomer can result in non-specific interactions, whereas a low amount of monomer can lead to a lower density of specific recognition sites. A compromise was reached at an M/BG ratio of 8/1. This ratio falls within the commonly employed range of 4/1 to 16/1 for non-covalent interactions and has been demonstrated to enhance selectivity in previous investigations [5].

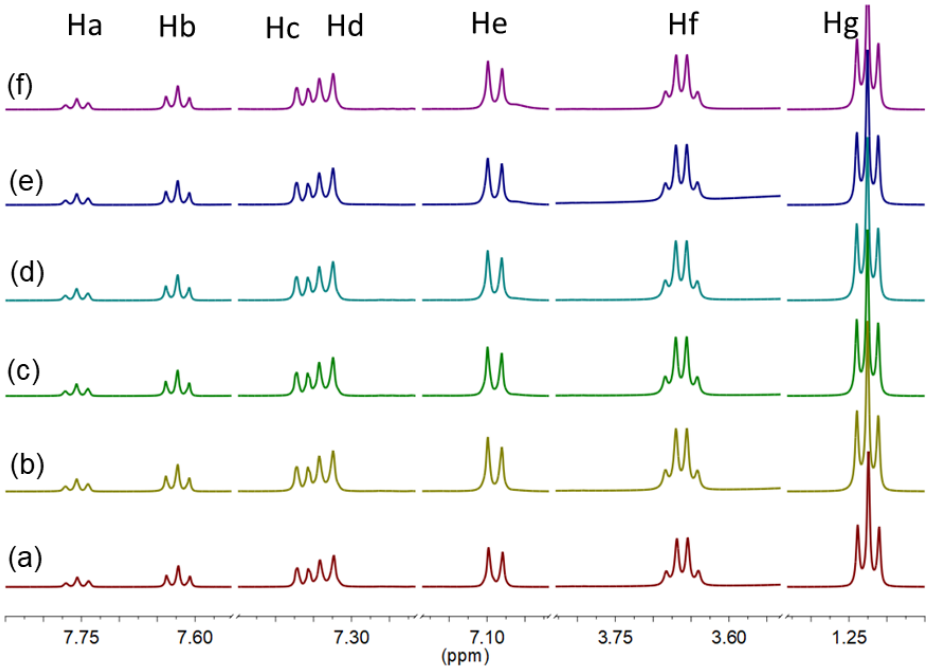

Figure 9. ^{1}H NMR spectra of BG at a constant concentration of 1.2 10^{-2} mol·L^{-1} in the presence of different concentrations of AA: (a) pure BG, and BG/AA molar ratio of 1/4, 1/6, 1/8, 1/10 and 1/12 in DMSO-d_6.

3.3.1. Detection of interactions with NOESY 2D NMR

Furthermore, the confirmation of the BG/AA interaction was obtained through the NOESY 2D NMR technique. The 2D NOESY contour plot showed correlation peaks for all protons of BG and AA, specifically for a BG/AA molar ratio of 1/8 (Fig. 10). The most intense correlation peaks were observed between the He protons of BG and the Hk, Hl and Hm protons of AA, indicating their close proximity. These strong correlation peaks suggest the presence of π-π interactions between the vinyl part of AA and the phenyl group of BG, as well as hydrogen bonding between the amino group of AA and the amino group of BG. This proposed structure of the complex aligns with the idea of an additional interaction between the phenyl group of BG and the vinyl group of AA through π-stacking.

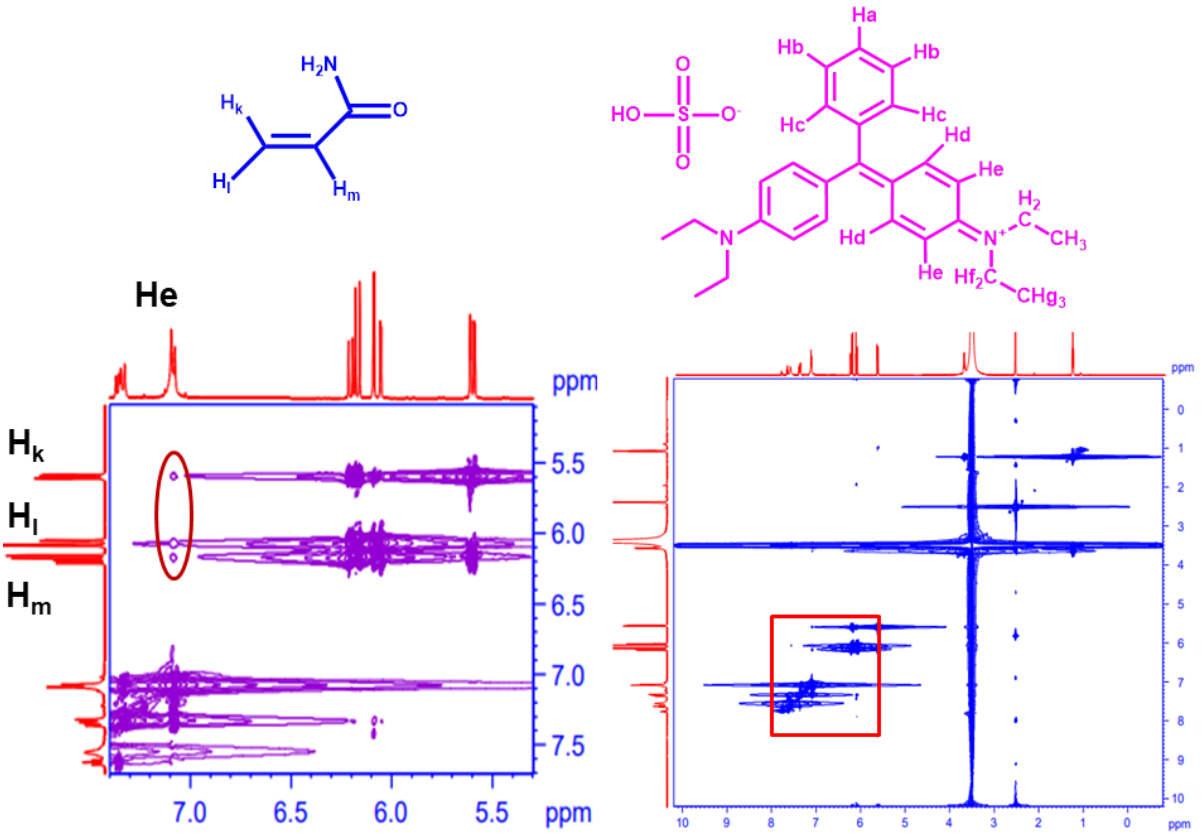

Figure 10. 2D NOESY spectrum of BG/AA mixed solution at a 1/8 mole ratio in DMSO-d_6.

3.3.2. Determination of the stoichiometry of complex species

In order to determine the stoichiometry and stability constant of the complexes formed in the pre-polymerization medium between the functional monomer (M) and the template molecule (T), the continuous variation or Job's method [17] was employed. In this method, the total concentration of (M) and (T) is kept constant. The maximum $r\Delta\delta$ for the protons of BG, as well as $(1-r)\Delta\delta$ for MAA at r = 0.5, indicates a 1:1 stoichiometry (Fig. S9). The quantitative determination of the association constant was performed by an exact calculation of Job's plot using the definition of the association constant and the material balance of BG and MAA. The 1:1 model was fitted to the experimental data, resulting in an association constant K_1 equal to 963 for the BG:MAA complex. In the case of the BG:AA complex, fitting to a 1:1 or 1:2 model alone was not satisfactory. However, Job plot analysis showed a clear preference for the 1:2 complexation model with a slight contribution from a 1:1 complex. The maximum $r\Delta\delta$ is observed for the BG protons at r = 0.33 (Fig. 11) and for the AA protons, the maximum $(1-r)\Delta\delta$ is obtained at r = 0.66 (Fig. S10). The first association constant K_1 = 40 is much smaller than the second constant K_2 = 9000.

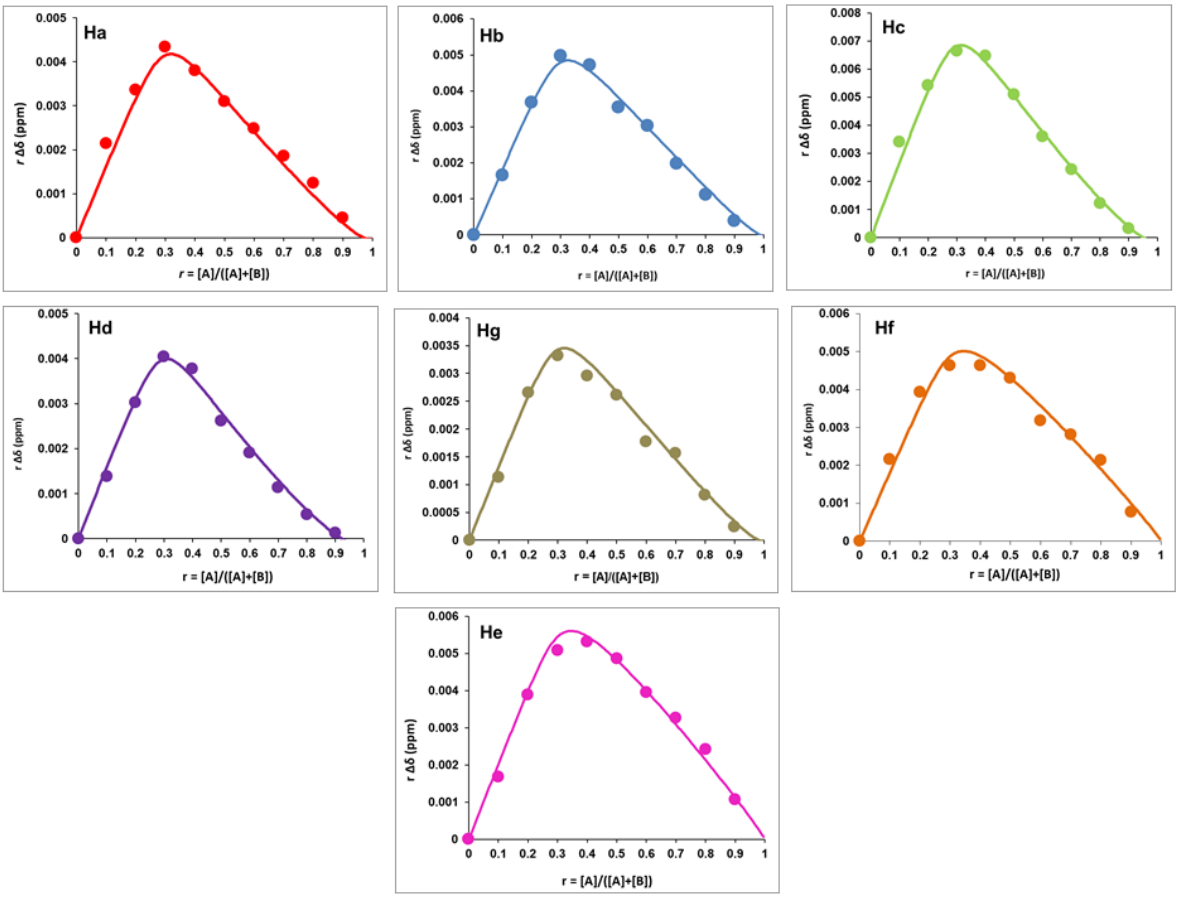

Figure 11. Job plots for the chemical shifts of Ha, Hb, Hc, Hd, He, Hf, and Hg protons in the BG:AA_2 complex.

Table 4. Stoichiometry and association constants of the complexes between Brilliant Green and the monomers in DMSO-d_6.

Complex system	Stoichiometry	K_1	K_2
BG:MAA	1:1	963 ± 0.04	–
BG:AA_2	1:1	40 ± 0.01	9000 ± 0.01

3.3.3. General Discussion

Methacrylic acid is the most commonly used functional monomer for the fabrication of MIPs. It is an acid that can strongly interact with bases and acts as a hydrogen bond donor. In the case of a basic molecule such as Brilliant Green, the interactions with the acid groups of MAA and its (co)polymers are expected strong. However, in the case of too strong acidic and basic groups, a H^+ ion is transferred from the carboxylic acid to the amino group of BG because an acid-base chemical reaction occurs. The actual chemical species that interact are the products of such acid-base reaction, which are a weak base (carboxylate anion) and a weak acid (ammonium cation). Hydrogen bond interactions are still possible, but they are much weaker than expected

[17]. The acid-base reaction produces oppositely charged ionic species that can bind through electrostatic interactions that cannot achieve selective binding because they are neither directional nor specific. The ammonium cation, potentially bound to the carboxylate anion of the MIP through electrostatic interactions, can be ion-exchanged with any cation (e.g., Na^+) present in the liquid medium. A functional monomer with weakly acidic groups may be preferred to MAA. This study selected acrylamide (AA) as a weakly acidic functional monomer. Acrylamide monomers have been found to be effective in providing selectivity to MIP materials for carboxylic anionic targets [17,38]. Brilliant Green possesses two amino groups with p*K*a values of 2.62 and 4.93. In acidic medium, the nitrogen of the amino group with a p*K*a ≈ 2.62 converts into an ammonium cation, while the nitrogen of the amino group adjacent to the imine function with a p*K*a ≈ 4.93 converts into an iminium cation. The most acidic group of acrylamide is the NH_2 of the primary amide group (with a p*K*a of 7.9 [39]). These functional groups interact with each other during the formation of molecular imprints. Based on this, the hydrogen bonding between BG and AA occurs between the protonated forms of BG at its amine group. Hydrogen bond interactions are currently considered because they are the strongest in the classification of intermolecular interactions. Illustrative scheme of the hydrogen bonding interactions of BG with AA and MAA are given in Fig. 12.

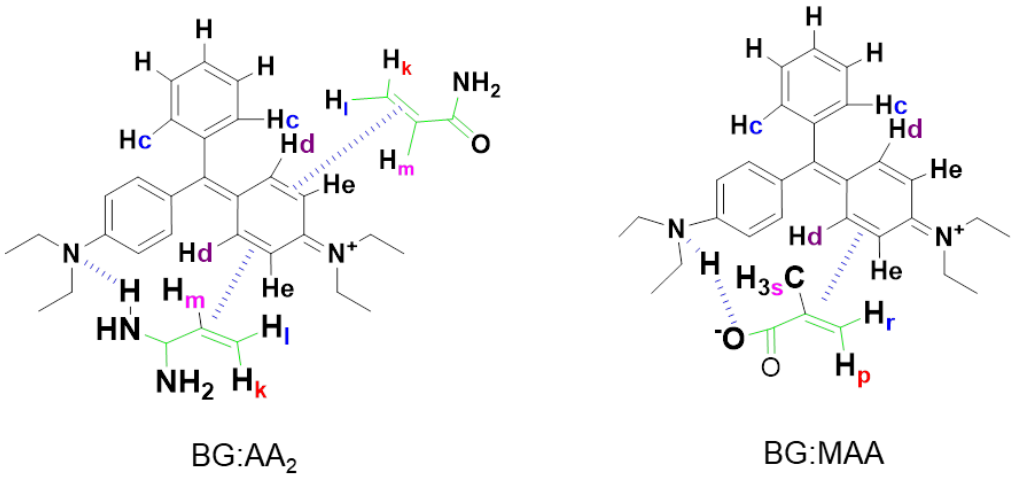

Figure 12. Illustrative scheme of intermolecular interactions of BG with AA and MAA.

3.5. Selectivity

The ability of an adsorbent to effectively differentiate and quantify the target analyte, even when other interfering molecules or metabolites are present in the sample is influenced by the arrangement of binding sites and the orientation of functional groups within the binding sites. Brilliant Green metabolites Eosine and Methylene Blue (Fig. S11) were chosen as potential

competitors for adsorption in a selectivity assessment. The characteristic parameters *D* and *α*, which represent the competitive adsorption, were calculated using Eqs 18 and 19, respectively, and are presented in Table 5. The distribution coefficient of Brilliant Green in all the prepared MIPs was significantly higher than that of its competitors, especially for PosAA@MIP (Fig. S12). The specific binding sites created on the imprinted polymer surface allow the discrimination of template molecules based on their shape, size, distribution and orientation of functional groups. PosAA@MIP showed higher extraction efficiency for Brilliant Green compared to PosMAA@MIP. The competing molecules closely resemble Brilliant Green in terms of structural similarity, particularly due to the presence of aromatic rings. However, they can be differentiated by the presence of sulfide (BM) or carboxylic and phenolic groups (Eos). In the case of MIPs, the values of selectivity coefficient *α* with respect to Brilliant Green were high. This showed that the molecular imprints created by the BG template were not suitable for accommodating Eosin and Methylene Blue.

Table 5. Extraction efficiencies (*ee*), distribution coefficients (*D*) and selectivity coefficients (*α*) of imprinted materials.

Molecules	PosMAA@MIP			PosMAA@NIP			PosAA@MIP			PosAA@NIP		
	ee (%)	*D* ($L \cdot g^{-1}$)	*α*	*ee* (%)	*D* ($L \cdot g^{-1}$)	*α*	*ee* (%)	*D* ($L \cdot g^{-1}$)	*α*	*ee* (%)	*D* ($L \cdot g^{-1}$)	*α*
Brilliant Green (BG)	89.6	4.34	–	57.0	0.66	–	95.7	11.1	–	51.0	0.52	–
Eosin (Eos)	60.4	0.76	6	53.3	0.67	1	65.4	0.94	11	54.3	0.59	0.9
Methylene Blue (MB)	63.6	0.87	5	54.7	0.60	1	67.6	1.04	10	55.7	0.62	0.8

4. Conclusion

Molecularly imprinted materials have been successfully synthesized using the biomaterial Posidonia as a robust support. The actual presence of selective molecular imprints is shown by the higher amounts of BG adsorbed on MIP than on NIP over the whole concentration range of the adsorption isotherm (Fig. 8) and the selective adsorption of BG compared to its metabolites (Table 5). Coating the MIP as a thin film on the surface of a solid support met the expectations of fast adsorption and higher selectivity. The acrylamide functional monomer showed better performance for selective adsorption than the methacrylic acid, in agreement with its stronger hydrogen bonding association with BG in solution. In fact, as shown by Boukadida et al. [17], although hydrogen bonds is based on acid-base interactions, a strong acid undergoes a proton transfer to the base rather than sharing the proton in an acid-base hydrogen bond. Acrylamide

as a functional monomer is an alternative to the widely used methacrylic acid seen as a 'universal' functional monomer in various applications such as analytical chemistry and environmental remediation. The clear advantages of using acrylamide-based MIPs in selective adsorption applications have been illustrated in several cases for the extraction of toxins (histamine) [17,40] and proteins (haemoglobin) [41]. A robust thermodynamic analysis using the Volmer adsorption isotherm outperformed the conventional Langmuir isotherm, providing a more realistic account of the mobility of non-specifically adsorbed molecules. The Langmuir-Volmer model, which fitted well to the experimental data, highlighted specific imprinted sites on the MIPs, which exhibited higher adsorption capacities compared to non-imprinted polymers (NIPs). Posidonia fibers are suitable solid supports for MIPs. Posidonia is a biosourced sustainable material that can be easily modified by chemical grafting. Its use is a valorization of a waste collected each spring to clean the beaches before the summer tourist season. This innovative approach demonstrates the potential of MIPs coated on solid supports from biomass to selectively extract BG from complex environmental media and provide enriched extracted media for quantitative analysis of trace amounts collected in the environment.

Declaration of interests

The authors declare that they have no known competing financial interests or personal relationships that could have appeared to influence the work reported in this paper.

Acknowledgments

This work was supported by the Cross-border project Italy–Tunisia "Méthodologies d'Économie Durable pour les déchets Côtiers Utilisables des Plages" (MEDDé.Co.U.Plages IS_3.2_086).

References

[1] Enache A.-C., Cojocaru C., Samoila P., Ciornea V., Apolzan R., Predeanu G., Harabagiu V. Adsorption of Brilliant Green dye onto a mercerized biosorbent: Kinetic, thermodynamic, and molecular docking studies. *Molecules* **2023**, *28*, 4129, doi:10.3390/molecules28104129.

[2] Babalska Z.Ł., Korbecka-Paczkowska M., Karpiński T.M. Wound antiseptics and European Guidelines for antiseptic application in wound treatment. *Pharmaceuticals* **2021**, *14*, 1253, doi:10.3390/ph14121253.

[3] Sharma J., Sharma S., Soni V. Toxicity of malachite green on plants and its phytoremediation: a review. *Reg. Stud. Mar. Sci.* **2023**, *62*, 102911, doi:10.1016/j.rsma.2023.102911.

[4] Sudova E., Machova J., Svobodova Z., Vesely T. Negative effects of malachite green and possibilities of its replacement in the treatment of fish eggs and fish: a review. *Vet. Med. Czech.* **2007**, *52*, 527–539, doi:10.17221/2027-VETMED.

[5] Tom L., Schneck N., Walter C. Improving the imprinting effect by optimizing template:monomer:cross-linker ratios in a molecularly imprinted polymer for sulfadimethoxine. *J. Chromatogr. B* **2012**, *909*, 61–64, doi:10.1016/j.jchromb.2012.10.020.

[6] Kumari N., Chintakula S., Anantha I.S.S., Maddila S. An efficient P3TA/Fe doped TiO_2 catalyst for photo-degradation of Brilliant green dye and inactivation of pathogens under visible light. *Results Chem.* **2023**, *5*, 100759, doi:10.1016/j.rechem.2022.100759.

[7] Mathiyalagan S., Mandal B.K., Ling Y.-C. Determination of synthetic and natural colorants in selected green colored foodstuffs through reverse phase-high performance liquid chromatography. *Food Chem.* **2019**, *278*, 381–387, doi:10.1016/j.foodchem.2018.11.077.

[8] López-Gutiérrez N., Romero-González R., Plaza-Bolaños P., Martínez-Vidal J.L., Garrido-Frenich A. Simultaneous and fast determination of Malachite Green, Leucomalachite Green, Crystal Violet, and Brilliant Green in seafood by ultrahigh performance liquid chromatography–tandem mass spectrometry. *Food Anal. Methods* **2013**, *6*, 406–414, doi:10.1007/s12161-012-9456-9.

[9] Somsen G.W., Coulter S.K., Gooijer C., Velthorst N.H., Brinkman U.A.Th. Coupling of column liquid chromatography and surface-enhanced resonance Raman spectroscopy via a thin-layer chromatographic plate. *Anal. Chim. Acta* **1997**, *349*, 189–197, doi:10.1016/s0003-2670(97)00011-1.

[10] Ayadi C., Anene A., Kalfat R., Chevalier Y., Hbaieb S. Molecularly imprinted polyaniline on silica support for the selective adsorption of benzophenone-4 from aqueous media, *Colloids Surfaces A: Physicochem. Eng. Aspects* **2019**, *567*, 32–42, doi:10.1016/j.colsurfa.2019.01.042.

[11] Jaoued-Grayaa N., Nasraoui C., Chevalier Y., Hbaieb S. Design of molecularly imprinted polymer materials relying on hydrophobic interactions, *Colloids Surfaces A: Physicochem. Eng. Aspects* **2022**, *647*, 129008, doi:10.1016/j.colsurfa.2022.129008.

[12] Nasraoui C., Jaoued-Grayaa N., Vanoye L., Chevalier Y., Hbaieb S. Development of molecularly imprinted polymer for the selective recognition of the weakly interacting fenamiphos molecule, *Eur. Polym. J.* **2022**, *177*, 111441, doi:10.1016/j.eurpolymj.2022.111441.

[13] Yang, Y., Shen, X. Preparation and application of molecularly imprinted polymers for flavonoids: Review and perspective. *Molecules* **2022**, 27, 7355, doi:10.3390/molecules27217355.

[14] Babaeipour, V., Jabbari, F. Pre-polymerization process simulation, synthesis and investigation the properties of dipicolinic acid molecularly imprinted polymers. *Polym. Bulletin* **2024**, *81*, 1495–1512, doi:10.1007/s00289-023-04774-w.

[15] Anene A., Hosni K., Chevalier Y., Kalfat R., Hbaieb S. Molecularly imprinted polymer for extraction of patulin in apple juice samples, *Food Control* **2016**, *70*, 90–95, doi:10.1016/j.foodcont.2016.05.042.

[16] Hasanah A.N., Safitri N., Zulfa A., Neli N., Rahayu D. Factors affecting preparation of molecularly imprinted polymer and methods on finding template-monomer interaction as the key of selective properties of the materials. *Molecules* **2021**, *26*, 5612, doi:10.3390/molecules26185612.

[17] Boukadida M., Anene A., Jaoued-Grayaa N., Chevalier Y., Hbaieb S. Choice of the functional monomer of molecularly imprinted polymers: Does it rely on strong acid-base or hydrogen bonding interactions? *Colloid Interface Sci. Commun.* **2022**, *50*, 100669, doi:10.1016/j.colcom.2022.100669.

[18] Renny J.S., Tomasevich L.L., Tallmadge E.H., Collum D.B. Method of continuous variations: Applications of Job plots to the study of molecular associations in organometallic chemistry. *Angew. Chem. Int. Ed.* **2013**, *52*, 11998, doi:10.1002/anie.201304157.

[19] Kouki S., Jaoued-Grayaa N., Anene A., Beyou E., Chevalier Y., Hbaieb S. The enhanced adsorption properties of molecular imprinted polymer material prepared using nitroxide-mediated Radical Deactivation Reversible Polymerization, *Polymer* **2022**, *249*, 124841, doi:10.1016/j.polymer.2022.124841.

[20] Anene A., Kalfat R., Chevalier Y., Hbaieb S. Design of molecularly imprinted polymeric materials: The crucial choice of functional monomers. *Chem. Africa* **2020**, *3*, 769–781, doi:10.1007/s42250-020-00180-1.

[21] Chianella I., Karim K., Piletska E.V., Preston C., Piletsky S.A. Computational design and synthesis of molecularly imprinted polymers with high binding capacity for pharmaceutical applications-model case: Adsorbent for abacavir. *Anal. Chim. Acta* **2006**, *559*, 73–78, doi:10.1016/j.aca.2005.11.068.

[22] Sullivan M.V., Dennison S.R., Hayes J.M., Reddy S.M. Evaluation of acrylamide-based molecularly imprinted polymer thin-sheets for specific protein capture–a myoglobin model. *Biomed. Phys. Eng. Express* **2021**, *18*, 45025, doi:10.1088/2057-1976/ac0991.

[23] Hutchins K.M. Functional materials based on molecules with hydrogen-bonding ability: applications to drug co-crystals and polymer complexes. *R. Soc. Open. Sci.* **2018**, *27*, 180564, doi:10.1098/rsos.180564.

[24] Murdaya N., Triadenda A.L., Rahayu D., Hasanah A.N. A review: Using multiple templates for molecular imprinted polymer: Is It Good? *Polymers* **2022**, *14*, 4441, doi:10.3390/polym14204441.

[25] Pedicini R., Maisano S., Chiodo V., Conte G., Policicchio A., Agostino R.G. Posidonia Oceanica and Wood chips activated carbon as interesting materials for hydrogen storage. *Int. J. Hydrogen Energy* **2020**, *45*, 14038–14047, doi:10.1016/j.ijhydene.2020.03.130.

[26] Tarchoun F.A., Trache D., Klapötke M.T. Microcrystalline cellulose from *Posidonia oceanica* brown algae: Extraction and characterization. *Int. J. Biol. Macromol.* **2019**, *138*, 837–845, doi:10.1016/j.ijbiomac.2019.07.176.

[27] Hermans P.H., Weidinger A. Quantitative X-ray investigations on the crystallinity of cellulose fibers. A background analysis. *J. Appl. Phys.* **1948**, *19*, 491–506, doi:10.1063/1.1698162.

[28] Terinte N., Ibbett R., Schuster K.C. Overview on native cellulose and microcrystalline cellulose I structure studied by X-ray diffraction (WAXD): Comparison between measurement techniques. *Lenzinger Ber.* **2011**, *89*, 118–131.

[29] Gul S., Gul A., Gul H., Khattak R., Ismail M., Khan S.U., Khan M.S., Aouissi H.A., Krauklis A. Removal of Brilliant Green dye from water using *Ficus benghalensis* tree leaves as an efficient biosorbent. *Materials* **2023**, *16*, 521, doi:10.3390/ma16020521.

[30] Wang L., Zhi K., Zhang Y., Liu Y., Zhang L., Yasin A., Lin Q. Molecularly imprinted polymers for gossypol via sol-gel, bulk, and surface layer imprinting–A comparative study. *Polymers* **2019**, *11*, 602, doi:10.3390/polym11040602.

[31] Sellergren B., Hall A.J. Fundamental aspects of imprinted network polymers. In Sellergren B. (ed.) *Molecularly Imprinted Polymers. Man-made Mimics of Antibodies and their Applications in Analytical Chemistry*. Elsevier: Amsterdam, **2001**, Chap 2, pp 31–35.

[32] Tan J., Wang H.-F., Yan X.-P. Discrimination of saccharides with a fluorescent molecular imprinting sensor array based on phenylboronic acid functionalized mesoporous silica. *Anal. Chem.* **2009**, *81*, 5273–5280, doi:10.1021/ac900484x.

[33] Suedee R., Seechamnanturakit V., Suksuwan A., Canyuk B. Recognition properties and competitive assays of a dual dopamine/serotonin selective molecularly imprinted polymer. *Int. J. Mol. Sci.* **2008**, *9*, 2333–2356, doi:10.3390/ijms9122333.

[34] Pan J., Yao H., Guan W., Ou H., Huo P., Wang X., Zou X., Li C. Selective adsorption of 2,6-dichlorophenol by surface imprinted polymers using polyaniline/silica gel composites as functional support: Equilibrium, kinetics, thermodynamics modeling. *Chem. Eng. J.* **2011**, *172*, 847–855, doi:10.1016/j.cej.2011.06.072.

[35] Abd El-Aal M.A., Al-Ghobashy M.A., Fathalla F.A., El-Saharty Y.S. Preparation and characterization of pH-responsive polyacrylamide molecularly imprinted polymer: Application to isolation of recombinant and wild type human serum albumin from biological sources. *J. Chromatogr. B* **2017**, *1046*, 34–47, doi:10.1016/j.jchromb.2017.01.031.

[36] Nicholls I.A., Chavan S., Golker K., Karlsson B.C.G., Olsson G.D., Rosengren A.M., Suriyanarayanan S., Wiklander J.G. Theoretical and computational strategies for the study of the molecular imprinting process and polymer performance. In: Mattiasson B., Ye L. (eds), Molecularly Imprinted Polymers in Biotechnology, *Adv. Biochem. Eng. Biotechnol.* Springer:*Cham*, **2015**, *150*, 25–50, doi:10.1007/10_2015_318.

[37] Qader B., Hussain I., Baron M., Jimenez-Perez R., Gonzalez-Rodriguez J., Gil-Ramírez R. A molecular imprinted polymer sensor for biomonitoring of fenamiphos pesticide metabolite fenamiphos sulfoxide. *Electroanalysis* **2021**, *33*, 1129–1136, doi:10.1002/elan.202060599.

[38] Urraca J.L., Hall A.J., Moreno-Bondi M.C., Sellergren B. A stoichiometric molecularly imprinted polymer for the class-selective recognition of antibiotics in aqueous media. *Angew. Chem. Int. Ed.* **2006**, *45*, 5158–5161, doi:10.1002/anie.200601636.

[39] Madhavan V., Lichtin N.N., Hayon E. Protonation reactions of electron adducts of acrylamide derivatives. A pulse radiolytic-kinetic spectrophotometric study. *J. Am. Chem. Soc.* **1975**, *97*, 2989–2995, doi:10.1021/ja00844a013.

[40] Boukadida M., Jaoued-Grayaa N., Anene A., Chevalier Y., Hbaieb S. Effect of cross-linking agents on the adsorption of histamine on molecularly imprinted polyacrylamide. *Polymer* **2023**, *268*, 125724, doi:10.1016/j.polymer.2023.125724.

[41] El-Sharif H.F., Turner N.W., Reddy S.M., Sullivan M.V. Application of thymine-based nucleobase-modified acrylamide as a functional co-monomer in electropolymerised thin-film molecularly imprinted polymer (MIP) for selective protein (haemoglobin) binding. *Talanta* **2022**, *240*, 123158, doi:10.1016/j.talanta.2021.123158.

SUPPORTING INFORMATION

Posidonia based Molecularly Imprinted Polymers for the efficient recognition of Brilliant Green

S1. Characterization of the modified Posidonia

The grafting process performed in anhydrous toluene yields a dense monomolecular layer of organosilane attached to the Posidonia surface. The resulting Pos@MPTS material were characterized by IR spectroscopy, and thermogravimetric analysis.

The ATR-FTIR spectroscopy was used to analyze the modified Posidonia. The IR spectrum for the modified Pos@MPTS is shown in Fig. S1, which indicates the existence of a strong absorption band of the Posidonia and the distinctive bands caused by chemical grafting, including those of the coupling agent (γ-methacryloxypropyltrimethoxysilane). Hydroxy surface groups of Pos@MPTS have a characteristic low-intensity band corresponding to the νC–OH vibrator around 3300 cm^{-1} because a part of them participated in the grafting reaction. Evidence of binding of γ-MPTS was given by the characteristic band of carbonyl vibration νC=O around 1720 cm^{-1}. The vibrations of CH_2 and CH_3 elongations ranging from 2960 to 2850 cm^{-1} confirmed the presence of organic compounds [1].

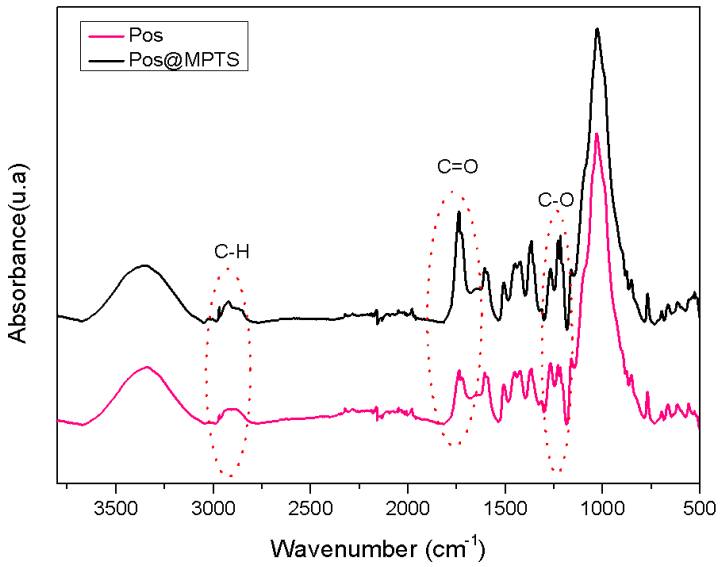

Figure S1. IR spectra of Pos and Pos@MPTS.

The grafting density of Pos@MPTS was assessed by thermogravimetric analysis (Fig. 2S). The mass loss of this biomaterial occurs in 3 stages. The condensation of unreacted Si–OMe groups and their hydrolyzed form (Si–OH), together with the amount of water adsorbed on the Posidonia surface are responsible for the first mass loss at 200 °C. A second mass loss between 250 °C and 600 °C corresponded to the decomposition of the organic materials grafted to the Posidonia surface and the organic phase, hemicellulose, cellulose, and lignin of Posidonia [2]. The last mass loss appearing in the range of 400–1000 °C corresponds to the combustion of carbon residues [3].

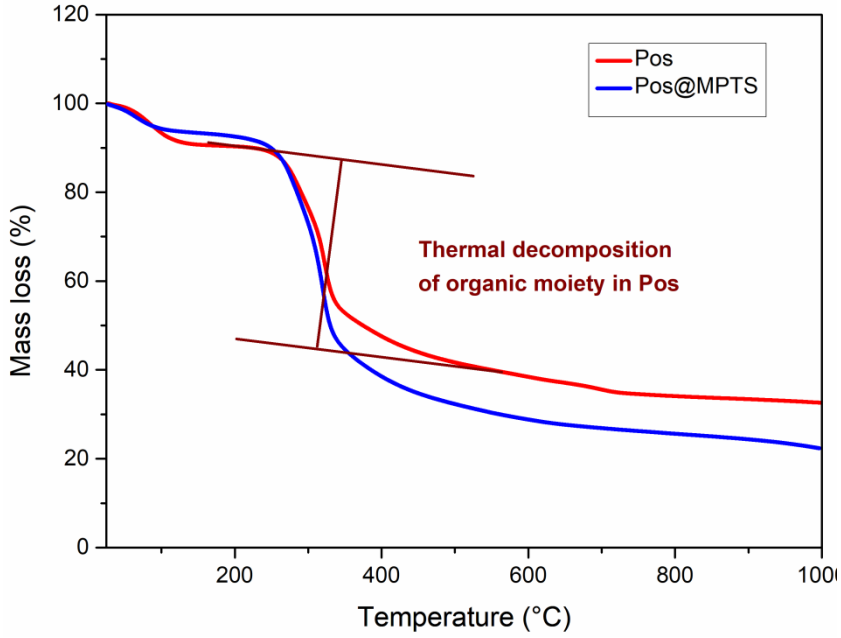

Figure S2. Thermogravimetric analysis of Pos and Pos@MPTS.

The grafting density was estimated from the recorded mass loss corresponding to the thermal decomposition of the organic graft occurring between 250 °C and 500 °C using Eq. S1:

$$d(\mu\text{mol}\cdot\text{g}^{-1}) = \frac{\frac{m(\text{Pos@MPTS})}{100-m(\text{Pos@MPTS})} - \frac{m(\text{Pos})}{100}}{M_{\text{mol}}(\text{MPTS})} \times 10^6 \qquad \text{(Eq. 1S)}$$

where m(Pos@MPTS) = 54.75% and m(Pos) = 49.09% are the mass losses of Pos@MPTS and Pos, M_{mol}(MPTS) = 128 g·mol^{-1} is the molar mass of the propylmethacryl moiety ($C_7H_{12}O_2$) lost upon thermal degradation [4]. The grafting density of γ-methacryloxypropyltrimethoxysilane on Posidonia surface was 5617 µmol·g^{-1}, which was close to the maximum grafting density of a dense close-packed monolayer of organosilane. If the coverage value is increased, it could result in a multilayer coating composed of organic species of γ-MPTS attached to the surface of Posidonia.

The X-ray diffraction (XRD) patterns of Pos, as shown in Fig. S3, exhibit characteristic diffraction peaks indicating the presence of amorphous cellulose. The peaks observed at 15.44 ° and 16.24 ° correspond to the primary equatorial planes (1$\bar{1}$0) and (110) of the monoclinic lattice. Additionally, the peak at 22.17 ° corresponds to the indexed primary equatorial plane (002), while the peak at 34.8 ° corresponds to the indexed primary equatorial plane (004). These findings provide confirmation of the presence of amorphous cellulose in the analyzed Posidonia sample. Amorphous cellulose is characterized by its lack of a well-defined crystalline structure, which aligns with the properties of Posidonia. The occurrence of amorphous cellulose in Posidonia can be attributed to the plant specific chemical composition and fibrous structure. These distinctive peaks are indicative of type I cellulose (monoclinic indexing) [3,5]. Based on these observations, it can be inferred that the crystallinity of Posidonia is influenced by the presence of amorphous cellulose.

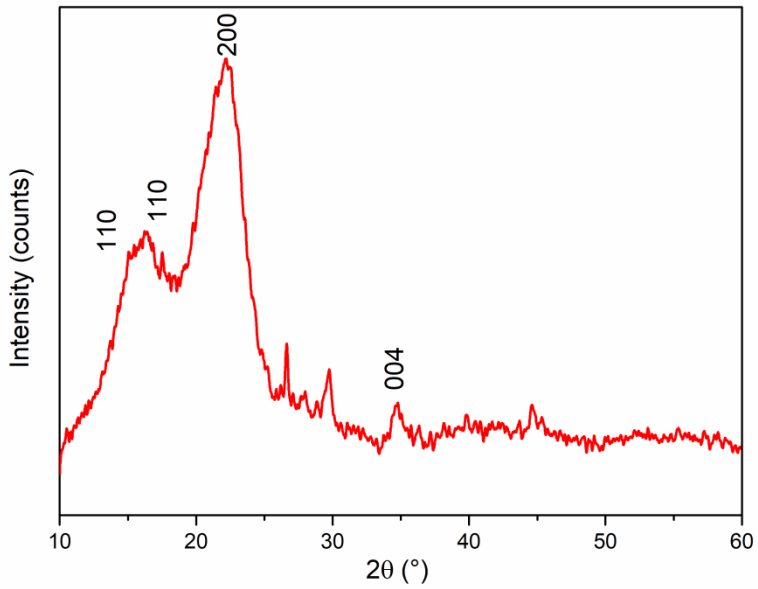

Figure S3. XRD pattern of Pos biomaterial.

S2. Adsorption as a function of pH

The adsorption behavior of molecules, including Brilliant Green, is influenced by the pH of the solution, as they can undergo ionization at different pH values [6]. In this study, the adsorption of Brilliant Green was investigated at four different pH values, 2, 4, 6 and 8. Due to its two p*K*a values of 2.0 and 4.9, Brilliant Green can exist in different ionization states within the pH range studied. The adsorption of Brilliant Green was found to be most favorable at pH 4 (Fig. S4). The adsorption percentage (%*A*) of Brilliant Green was calculated using the following equation (Eq. S2):

$$\%A = (C_0 - Ce)\frac{100}{C_0} \quad \text{(Eq. S2)}$$

where C_0 and C_e represent the initial and equilibrium concentrations of Brilliant Green, respectively.

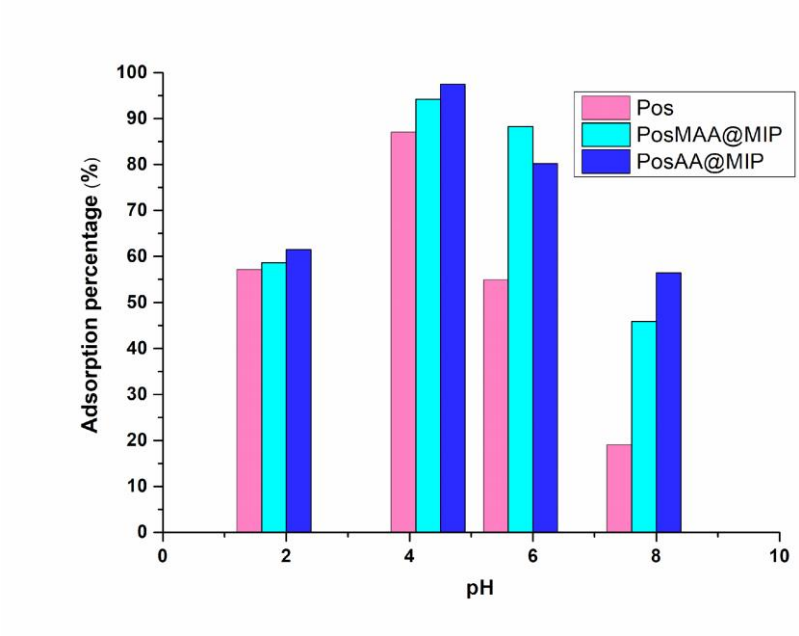

Figure S4. Adsorption percentage of BG at a concentration of 5 10^{-5} mol·L^{-1} onto Pos, PosMAA@MIP and PosAA@MIP at pH 2, 4, 6, 8 and 298 K.

S3. NMR study

The protons of Brilliant Green observed in NMR are illustrated in Fig. S5.

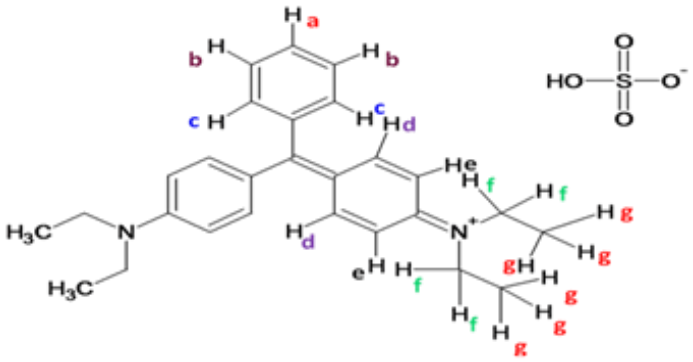

Figure S5. Structure of Brilliant Green.

The ^{1}H NMR spectra (Figs S6, S7 and S8) show the chemical shift values of the protons of BG, MAA and AA in DMSO-d_6.

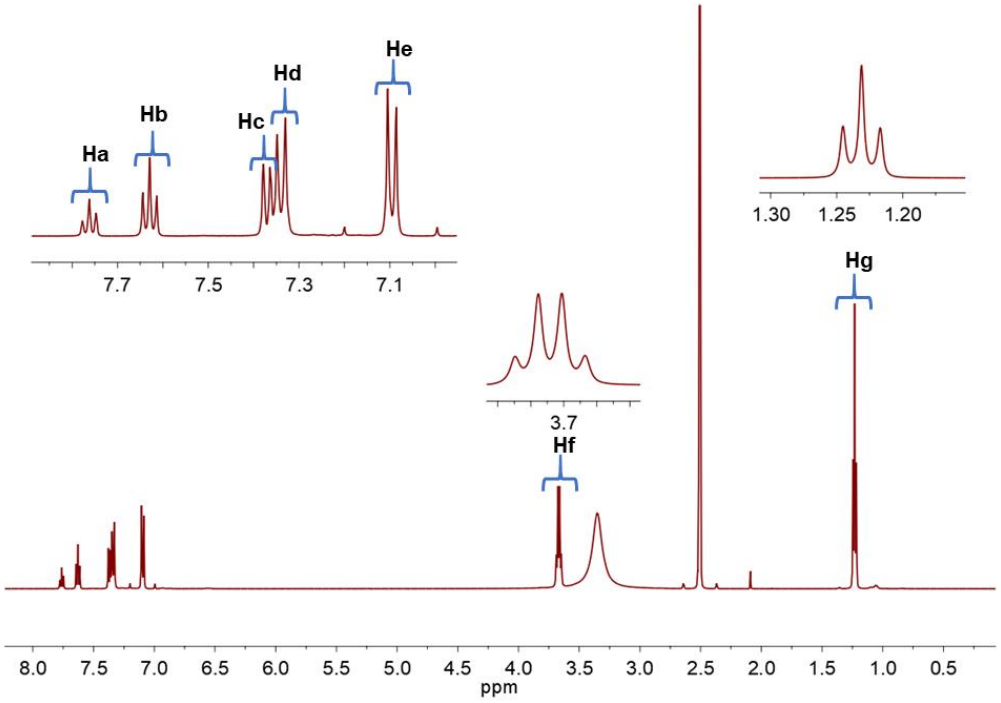

Figure S6. ^{1}H NMR spectrum of Brilliant Green in DMSO-d_6.

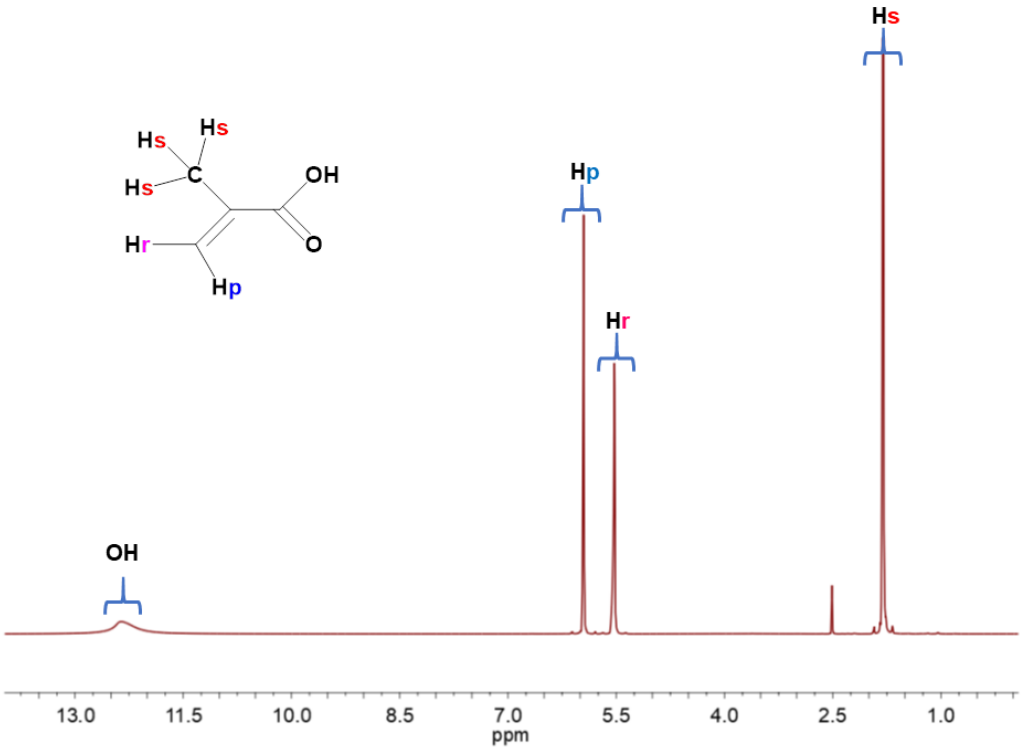

Figure S7. ^{1}H NMR spectrum of MAA in DMSO-d_6.

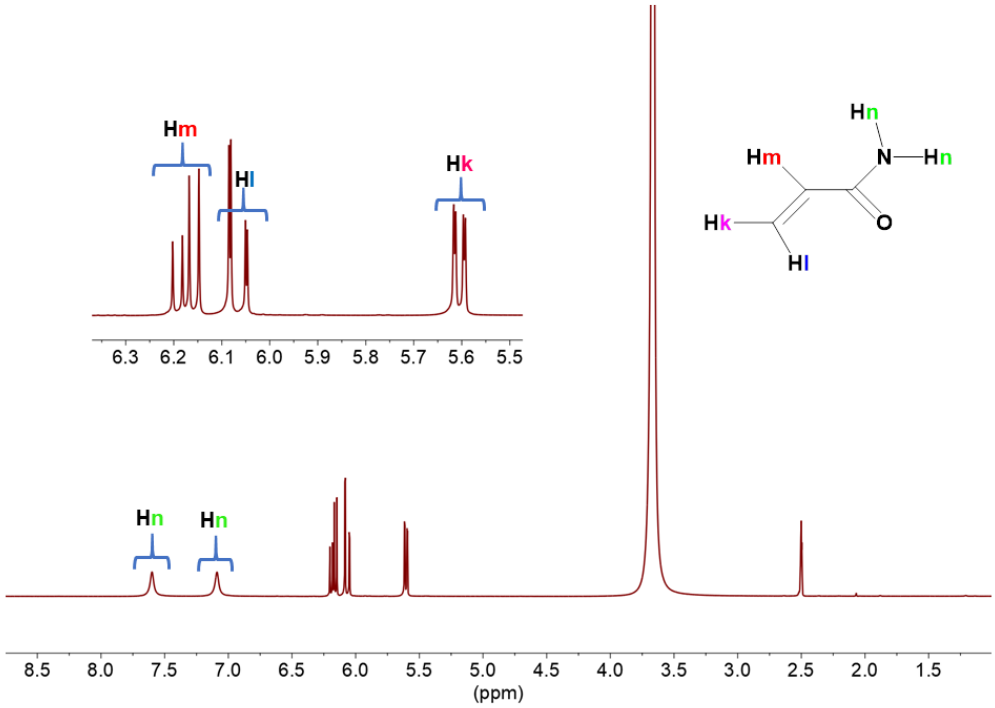

Figure S8. ^{1}H NMR spectrum of AA in DMSO-d_6.

The ^{1}H NMR spectrum (Fig. S9) shows the chemical shift variation of the protons of BG in the presence of different concentrations of MAA in DMSO-d_6.

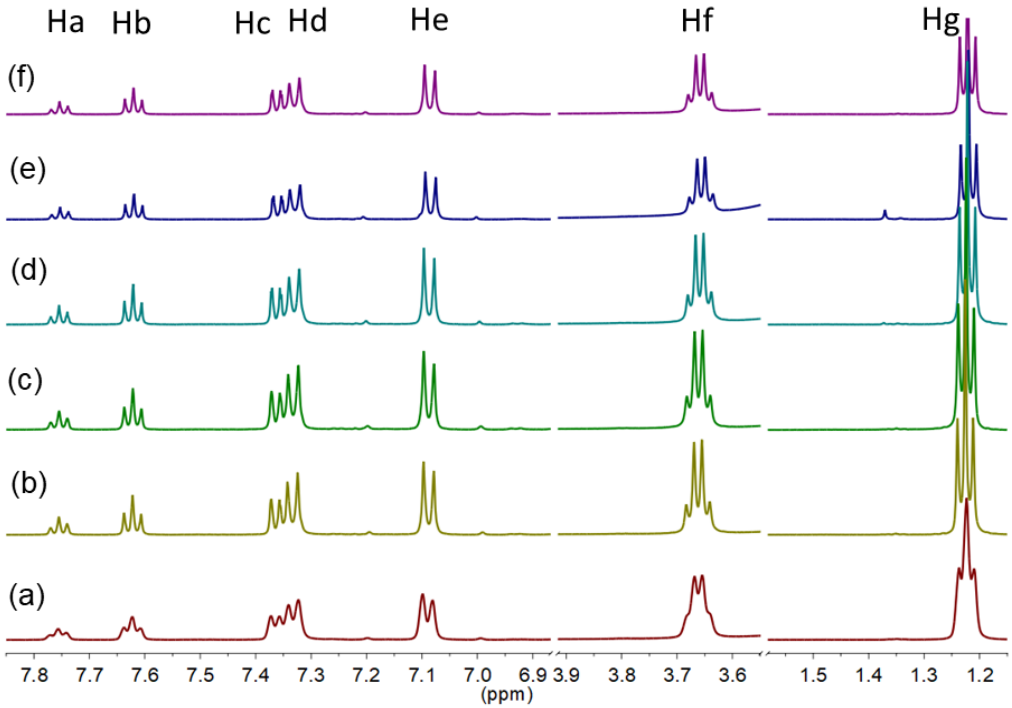

Figure S9. ^{1}H NMR spectra of BG at a constant concentration of 1.2 10^{-2} mol·L^{-1} in the presence of different concentrations of MAA: (a) pure BG, and BG/MAA molar ratio of 1/4, 1/6, 1/8, 1/10 and 1/12 in DMSO-d_6.

Table S1. ^{1}H NMR chemical shifts (ppm) of Ha, Hb, Hc, Hd, He, Hf and Hg protons of BG, either pure or in presence of the MAA functional monomer in DMSO-d_6.

MAA/BG mole ratio	Hg	Hf	He	Hd	Hc	Hb	Ha
0	1.2244	3.6615	7.0886	7.3325	7.3643	7.6221	7.7553
4	1.2246	3.6614	7.0879	7.3322	7.3645	7.6219	7.7550
6	1.2252	3.6611	7.0875	7.3323	7.3639	7.6214	7.7548
8	1.2268	3.6604	7.0871	7.3322	7.3621	7.6209	7.7547
10	1.2217	3.6605	7.0875	7.3351	7.3622	7.6209	7.7550
12	1.2214	3.6606	7.0879	7.3331	7.3625	7.6201	7.7549

Table S2. ^{1}H NMR chemical shifts (ppm) of Ha, Hb, Hc, Hd, He, Hf and Hg protons of BG, either pure or in presence of the AA functional monomer in DMSO-d_6.

AA/BG mole ratio	Hg	Hf	He	Hd	Hc	Hb	Ha
0	1.2244	3.6615	7.0886	7.3325	7.3643	7.6221	7.7553
4	1.2255	3.6626	7.0886	7.3334	7.3648	7.6230	7.7560
6	1.2256	3.6629	7.0899	7.3335	7.3650	7.6230	7.7563
8	1.2256	3.6629	7.0899	7.3355	7.3650	7.6231	7.7563
10	1.2256	3.6627	7.0896	7.3335	7.3649	7.6229	7.7560
12	1.2254	3.6625	7.0894	7.3333	7.3648	7.6228	7.7559

Table S3. ^{1}H NMR chemical shifts (ppm) of Ha, Hb, Hc, Hd, He, Hf and Hg protons of BG, as function as r = [BG] / ([BG] + [AA]) in DMSO-d_6.

[AA] (mM)	[BG] (mM)	r	Ha	Hb	Hc	Hd	Hg	Hf	He
26.16	0	0	7.7562	7.6226	7.3647	7.3317	1.2232	3.6614	7.0898
23.54	2.61	0.1	7.7538	7.6207	7.3610	7.3302	1.2219	3.6590	7.0880
20.93	5.23	0.2	7.7520	7.6180	7.3580	7.3280	1.2199	3.6565	7.0850
18.31	7.85	0.3	7.7500	7.6155	7.3553	7.3260	1.2184	3.6548	7.0826
15.7	10.46	0.4	7.7498	7.6147	7.3540	7.3255	1.2183	3.6537	7.0810
13.08	13.08	0.5	7.7500	7.6155	7.3546	7.3266	1.2180	3.6528	7.0801
10.46	15.7	0.6	7.7500	7.6150	7.3558	7.3270	1.2188	3.6535	7.0800
7.85	18.31	0.7	7.7500	7.6160	7.3567	7.3280	1.2180	3.6520	7.0790
5.23	20.93	0.8	7.7499	7.6170	7.3586	7.3291	1.2191	3.6507	7.0777
2.61	23.54	0.9	7.7516	7.6187	7.3615	7.3305	1.2207	3.6537	7.0791
0	26.16	1	–	–	–	–	–	–	–

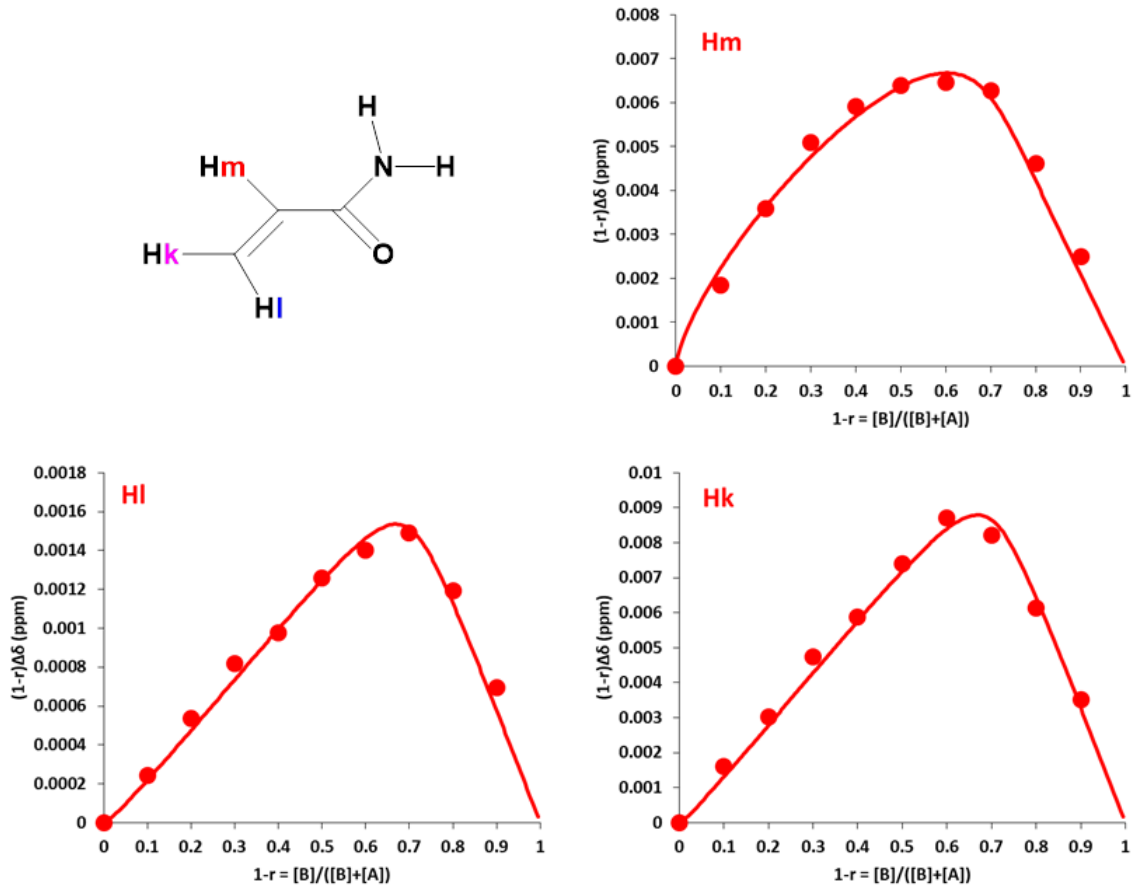

Figure S10. Job plots for the chemical shifts of AA protons in the complex BG:AA_2.

Table S4. ^{1}H NMR chemical shifts (ppm) of Ho, Hm, Hl, and Hk protons of AA as a function of $1 - r$ = [AA] / ([BG] + [AA]) in DMSO-d_6.

[AA] (mM)	[BG] (mM)	$1 - r$	Hm	Hl	Hk
26.16	0	0	–	–	–
23.54	2.61	0.1	6.2000	6.0610	5.6400
20.93	5.23	0.2	6.1980	6.0620	5.5740
18.31	7.85	0.3	6.1958	6.0630	5.5773
15.7	10.46	0.4	6.1911	6.0644	5.5830
13.08	13.08	0.5	6.1877	6.0654	5.5900
10.46	15.7	0.6	6.1848	6.0663	5.5950
7.85	18.31	0.7	6.1822	6.0668	5.5980
5.23	20.93	0.8	6.1794	6.0673	5.6010
2.61	23.54	0.9	6.1770	6.0677	5.6030
0	26.16	1	6.1749	6.0679	5.6047

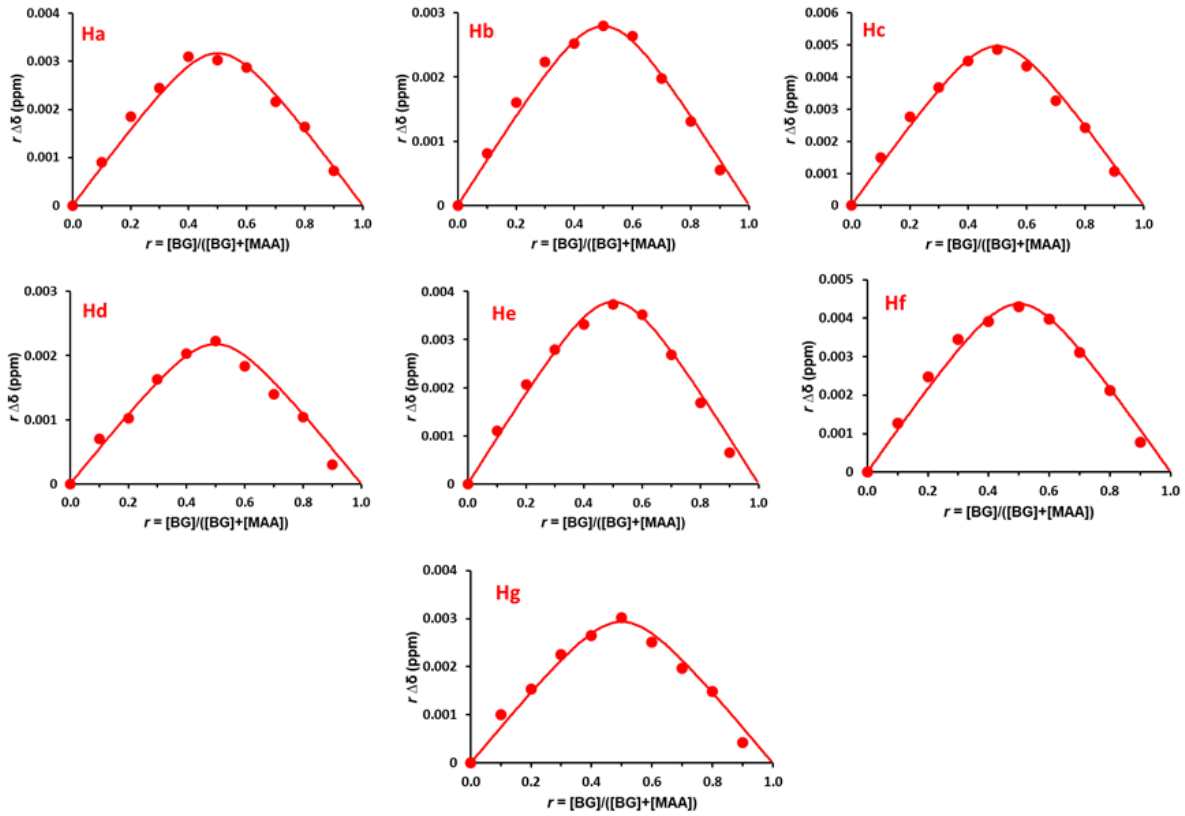

Figure S11. Job plots for the chemical shifts of BG protons in the complex BG:MAA.

Table S5. ^{1}H NMR chemical shifts (ppm) of Ha, Hb, Hc, Hd, He, Hf and Hg protons of BG, as function as *r* = [BG] / ([BG] + [MAA]) in DMSO-d_6.

[MAA] (mM)	[BG] (mM)	*r*	Hg	Hf	He	Hd	Hc	Hb	Ha
26.16	0	0	1.2232	3.6614	7.0898	7.3317	7.3648	7.6226	7.7562
23.54	2.61	0.1	1.2221	3.6600	7.0882	7.3310	7.3636	7.6217	7.7552
20.93	5.23	0.2	1.2213	3.6583	7.0864	7.3305	7.3622	7.6206	7.7538
18.31	7.85	0.3	1.2200	3.6565	7.0846	7.3295	7.3608	7.6194	7.7527
15.70	10.46	0.4	1.2188	3.6549	7.0824	7.3284	7.3593	7.6184	7.7510
13.08	13.08	0.5	1.2172	3.6528	7.0801	7.3273	7.3573	7.6170	7.7501
10.46	15.7	0.6	1.2170	3.6514	7.0790	7.3272	7.3560	7.6160	7.7490
7.85	18.31	0.7	1.2167	3.6510	7.0790	7.3271	7.3558	7.6160	7.7490
5.23	20.93	0.8	1.2158	3.6507	7.0777	7.3266	7.3564	7.6161	7.7480
2.61	23.54	0.9	1.2189	3.6537	7.0791	7.3288	7.3582	7.6171	7.7490
0	26.16	1	–	–	–	–	–	–	–

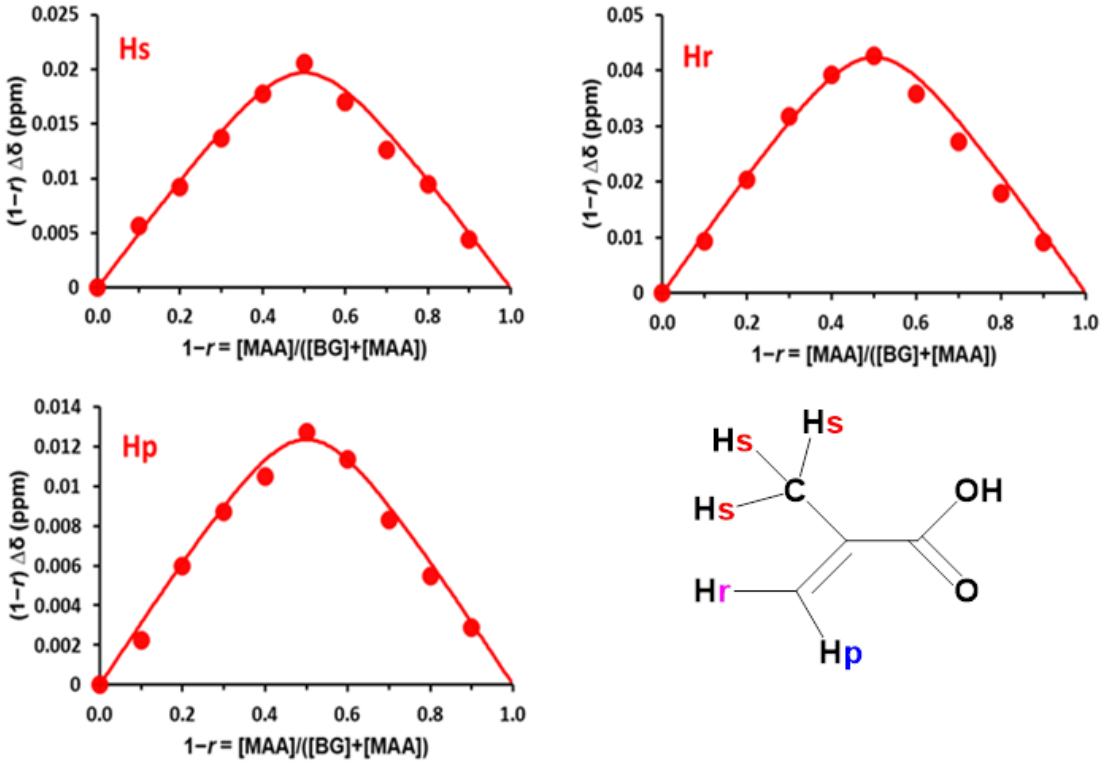

Figure S12. Job plots for the chemical shifts of MAA protons in the complex BG:MAA.

Table S6. ^{1}H NMR chemical shifts (ppm) of Hs, Hr, Hp, and Ho protons of MAA, as function as $1 - r$ = [MAA] / ([BG] + [MAA]) in DMSO-d_6.

[MAA] (mM)	[BG] (mM)	$1 - r$	Hs	Hr	Hp
26.16	0	0			
23.54	2.61	0.1	1.8345	5.6064	5.97124
20.93	5.23	0.2	1.8377	5.60461	5.969815
18.31	7.85	0.3	1.8325	5.60516	5.97025
15.7	10.46	0.4	1.8330	5.60428	5.97093
13.08	13.08	0.5	1.8315	5.6000	5.9680
10.46	15.7	0.6	1.8200	5.5800	5.9600
7.85	18.31	0.7	1.8100	5.5600	5.9550
5.23	20.93	0.8	1.8020	5.5400	5.9500
2.61	23.54	0.9	1.7967	5.525	5.945
0	26.16	1	1.79044	5.51463	5.94253

S4. Selectivity study

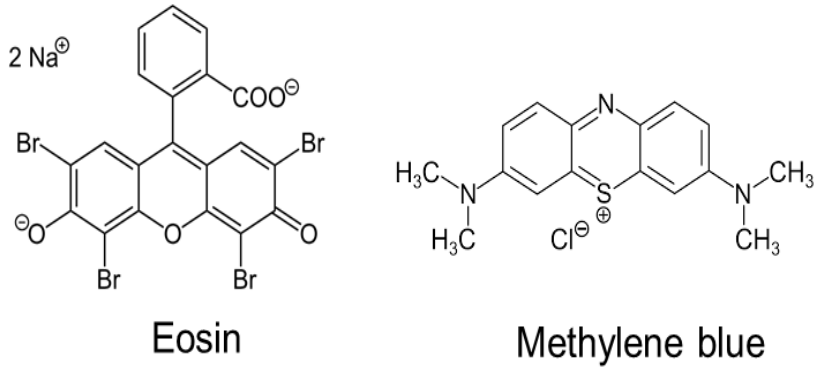

Figure S13. Chemical structures of metabolites of Brilliant Green.

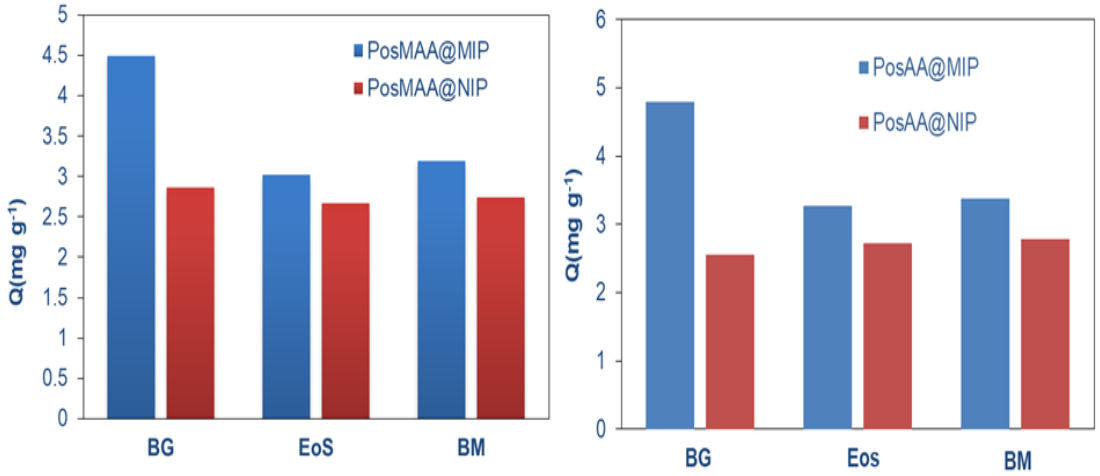

Figure S14. Binding capacities of PosAA@MIP and PANI@NIP for BP4, BP3 and BP.

References

[1] Boukadida M., Anene A., Jaoued-Grayaa N., Chevalier Y., Hbaieb S. Choice of the functional monomer of molecularly imprinted polymers: Does it rely on strong acid-base or hydrogen bonding interactions? *Colloid Interface Sci. Commun.* **2022**, 50, 100669, doi:10.1016/j.colcom.2022.100669.

[2] Errais E. Réactivité de surface d'argiles naturelles. Étude de l'adsorption de colorants anioniques, Thèse de doctorat, Université de Strasbourg, 2011, 49–69.

[3] Tarchoun F.A., Trache D., Klapötke M.T. Microcrystalline cellulose from *Posidonia oceanica* brown algae: Extraction and characterization. *Int. J. Biol. Macromol.* **2019**, 138, 837–845, doi:10.1016/j.ijbiomac.2019.07.176.

[4] Calvez I., Szczepanski C.R., Landry V. Preparation and characterization of low gloss UV-curable coatings based on silica surface modification using an acrylate monomer, *Prog. Org. Coatings.* **2021**, 158, 106369, doi:10.1016/j.porgcoat.2021.106369.

[5] Aguir C., Farouk M.M. Chemical modification of Posidonia with cyclic anhydrides: effect of thermal stability, *Carbohydr. Res.* **2010**, 345, 264–269, doi:10.1016/j.carres.2009.11.006.

[6] Gul S., Gul A., Gul H., Khattak R., Ismail M., Khan S.U., Khan M.S., Aouissi H.A., Krauklis A. Removal of Brilliant Green dye from water using *Ficus benghalensis* tree leaves as an efficient biosorbent. *Materials (Basel)* **2023**, 16, 521, doi:10.3390/ma16020521.